Fraunhofer Institut
Techno- und
Wirtschaftsmathematik

O. Iliev, A. Mikelic, P. Popov

Fluid structure interaction problems in deformable porous media: Toward permeability of deformable porous media

Berichte des Fraunhofer ITWM, Nr. 65 (2004)

ISSN 1434-9973

Bericht 65 (2004)

Die Veröffentlichungen in der Berichtsreihe des Fraunhofer ITWM können bezogen werden über:

Fraunhofer-Institut für Techno- und
Wirtschaftsmathematik ITWM
Gottlieb-Daimler-Straße, Geb. 49

67663 Kaiserslautern
Germany

Telefon: +49 (0) 6 31/2 05-32 42
Telefax: +49 (0) 6 31/2 05-41 39
E-Mail: info@itwm.fraunhofer.de
Internet: www.itwm.fraunhofer.de

Vorwort

Das Tätigkeitsfeld des Fraunhofer Instituts für Techno- und Wirtschaftsmathematik ITWM umfasst anwendungsnahe Grundlagenforschung, angewandte Forschung sowie Beratung und kundenspezifische Lösungen auf allen Gebieten, die für Techno- und Wirtschaftsmathematik bedeutsam sind.

In der Reihe »Berichte des Fraunhofer ITWM« soll die Arbeit des Instituts kontinuierlich einer interessierten Öffentlichkeit in Industrie, Wirtschaft und Wissenschaft vorgestellt werden. Durch die enge Verzahnung mit dem Fachbereich Mathematik der Universität Kaiserslautern sowie durch zahlreiche Kooperationen mit internationalen Institutionen und Hochschulen in den Bereichen Ausbildung und Forschung ist ein großes Potenzial für Forschungsberichte vorhanden. In die Berichtreihe sollen sowohl hervorragende Diplom- und Projektarbeiten und Dissertationen als auch Forschungsberichte der Institutsmitarbeiter und Institutsgäste zu aktuellen Fragen der Techno- und Wirtschaftsmathematik aufgenommen werden.

Darüberhinaus bietet die Reihe ein Forum für die Berichterstattung über die zahlreichen Kooperationsprojekte des Instituts mit Partnern aus Industrie und Wirtschaft.

Berichterstattung heißt hier Dokumentation darüber, wie aktuelle Ergebnisse aus mathematischer Forschungs- und Entwicklungsarbeit in industrielle Anwendungen und Softwareprodukte transferiert werden, und wie umgekehrt Probleme der Praxis neue interessante mathematische Fragestellungen generieren.

Prof. Dr. Dieter Prätzel-Wolters
Institutsleiter

Kaiserslautern, im Juni 2001

FLUID STRUCTURE INTERACTION PROBLEMS IN DEFORMABLE POROUS MEDIA: TOWARD PERMEABILITY OF DEFORMABLE POROUS MEDIA

OLEG ILIEV, ANDRO MIKELIC, AND PETER POPOV

Abstract. In this work the problem of fluid flow in deformable porous media is studied. First, the stationary fluid-structure interaction (FSI) problem is formulated in terms of incompressible Newtonian fluid and a linearized elastic solid. The flow is assumed to be characterized by very low Reynolds number and is described by the Stokes equations. The strains in the solid are small allowing for the solid to be described by the Lame equations, but no restrictions are applied on the magnitude of the displacements leading to strongly coupled, nonlinear fluid-structure problem. Then, an asymptotic solution to the FSI problem is developed for a long channel geometry. Nonlinear Darcy-type upscaled equations for the y-averaged pressure in the channel are obtained. While upscaling the FSI problem under such general conditions for arbitrary pore geometry is unlikely, the result can be used to select parameters for numerical upscaling. Further, the microscale FSI problem is treated numerically by an iterative procedure which solves sequentially fluid and solid subproblems. Each of the two subproblems is discretized by finite elements and the fluid-structure coupling is reduced to an interface boundary condition. Numerical and asymptotic solutions are found to converge to each other, thus validating both the numerical solver and the analytical derivation. Numerical computations are also used to perform permeability computations for different geometries.

1. Introduction

Many important engineering applications such as ground water flow, reservoir engineering, various filtering devices used in chemical processing, to name a few, involve flow in deformable porous media [4]. The upscaling of deformable porous media consists of two different physical processes. At the microscopic (pore) level one has a deformable skeleton surrounded by a fluid. The solid is usually described by the Lamé equations of linear elasticity and the fluid by the Stokes equations.

In general the upscaling problem for poroelasticity medium is not separable even when the microscopic heterogeneity (the pores) is well separated. This is due to the fact that the skeleton can deform arbitrarily large due to different parameters such as macroscopic displacements, pressure and velocity. However, for large classes of poroelastic problems it is possible to derive macroscopic equations.

The problem has been first studied experimentally by Biot [6, 4] who formulated the macroscopic equations for the effective medium. The application of the asymptotic homogenization method [5, 21, 3, 23] has lead to theoretical justification of Biot's equation [1, 21, 18] along with appropriate cell problems from which the macroscopic parameters can be computed numerically. The macroscopic equations are derived under the assumption that the solid-fluid

Date: June 28, 2005.

Key words and phrases. fluid-structure interaction, deformable porous media, upscaling, linear elasticity, stokes, finite elements.

interface displacements are small compared to the pore size. This allows to apply interface conditions at the initial position of the fluid solid interface and important properties such as periodicity of the unit cell are preserved. A wide range of applications, for example, in soil acoustics fall within these limits. However, many other important engineering problems cannot be considered under such severe restrictions.

Under more relaxed assumptions [15] have derived a nonlinear macroscopic governing equations by assuming periodic media and allowing the interface displacements to be of the same order as the pore size. It is also assumed that the total deformation of a the unit-cell can be decomposed into a rigid-body motion of each unit cell after which the interface displacement become infinitely small in the new reference frame. Under certain symmetry assumptions of the unit cell prior to the deformation it is shown that macroscopic equations reduce to Biot's law.

The focus of this paper is the case when, due to problem parameters such as macroscopic pressure and displacement, the fluid-solid interface deforms considerably at the pore level. When the interface cannot be approximated by a rigid body motion of its initial position it is necessary to consider the Fluid-Structure Interaction (FSI) problem at pore level as a problem with an unknown interface. In this work, the governing equations of the FSI problem are first formulated at the microscale. Then an asymptotic solution is derived for the case of a long channel with elastic walls. A nonlinear Darcy-type equation is found for the flow rate which depends on the average pressure. Further, a numerical method for the FSI problem is developed and used to verify the analytical result. Based on the indication from the channel that the most important upscaling parameter is the average averaged an effective permeability of a 3D foam structure is also performed.

2. The microscopic governing equations

Before we present the fluid structure problem at the microscale we begin with a brief summary of the notation used, the formulation of the fluid, and solid problems alone. Consider a continuum body at the pore level. The material points in the body are associated with points $\mathbf{p}$ in $\mathbb{R}^3$. A body is defines as an open subset $\Omega \subset \mathbb{R}^3$. We denote the reference configuration by Ω_0 which represents the body before the deformation has begun and the deformed configuration by Ω. We will use $\mathbf{p}$ to denote material coordinates and $\mathbf{x}$ to denote spatial ones. Further, we are concerned with stationary processes so the both the Lagrangian fields associated with the solid are time independent as are the Eulerian ones for the fluid.

This paper will deal with linear elastic solids which undergo significant pore-level deformation and to properly account for the resulting interface conditions between the solid and the fluid it is necessary to use the correct stress measures. Thus, consider a continuous, irreversible deformation

$$\mathbf{x} = \mathsf{x}(\mathbf{p}),$$

so the reference and deformed configurations are connected by $\Omega = \mathbf{x}(\Omega_0)$. The deformation gradient is denoted by $\mathbf{F}$:

$$\mathbf{F}(\mathbf{p}) = \nabla \mathbf{x}(\mathbf{p}). \tag{1}$$

Further, the usual Cauchy stress tensor is denoted by $\mathbf{T}(\mathbf{x})$. Observe that it is a spatial field, defined on the deformed configuration of the solid. For the elasticity problem, the first Piola-Kirchhoff stress tensor $\mathbf{S}(\mathbf{p})$ is also needed. It is related to $\mathbf{T}(\mathbf{x})$ by the identity:

$$\mathbf{S}(\mathbf{p}) = \det(\mathbf{F}(\mathbf{p}))\mathbf{T}(\mathbf{x}(\mathbf{p}))\mathbf{F}^{-T}(\mathbf{p}). \tag{2}$$

The solid, fluid and the coupled, Fluid-Structure Interaction (FSI) problems are summarized next.

2.1. **Solid.** Let $\mathbf{u}(\mathbf{p})$ be the displacements in the solid domain:

$$\mathbf{u}(\mathbf{p}) = \mathbf{x}(\mathbf{p}) - \mathbf{p}, \tag{3}$$

and $\mathbf{E}(\mathbf{p})$ be the usual infinite small strain:

$$\mathbf{E}(\mathbf{p}) = \frac{1}{2}\left(\nabla\mathbf{u}(\mathbf{p}) + \nabla\mathbf{u}(\mathbf{p})^T\right). \tag{4}$$

We restrict our attention to linear elastic solids only, that is, solids for which:

$$\mathbf{S} = \mathsf{C} : \mathbf{E}, \tag{5}$$

where C is the fourth order elasticity tensor[1]. The last relation (5) is known as Hooke's law.

Then, given a body force $\mathbf{b}_0$ in the reference configuration, the boundary value problem for a linear elastic solid is stated (in the reference configuration) as follows: *Find* $\mathbf{u}(\mathbf{p})$ *such that*

$$\nabla \cdot (\mathsf{C} : \mathbf{E}) + \mathbf{b}_0 = \mathbf{0} \text{ in } \Omega_0, \tag{6}$$

with Dirichlet

$$\mathbf{u} = \hat{\mathbf{u}} \text{ on } \Gamma_0^D, \tag{7}$$

and/or Neumann

$$\mathbf{S}\mathbf{n}_0 = \hat{\mathbf{s}} \text{ on } \Gamma_0^N \tag{8}$$

boundary data, with the usual conditions $\Gamma_0^D \bigcap \Gamma_0^N = \varnothing$ *and* $\Gamma_0^D \bigcup \Gamma_0^N = \Gamma_0$.

As will be seen in Section 2.3, on the part of the solid boundary which is an interface with the fluid a Neumann-type interface condition similar to (8) will be given. Therefore when this interface undergoes large movement (compared to the pore size) it is necessary to formulate it using the correct stress measure.

2.2. **Newtonian fluid at low Reynolds number.** Newtonian fluids are best described using spatial fields. For stationary problems (the spatial description of all involved quantities is time independent), one has a velocity $\mathbf{v}(\mathbf{x})$ and correspondingly, the symmetric part of the velocity gradient, namely, the stretching tensor $\mathbf{D}(\mathbf{x})$ given by:

$$\mathbf{D}(\mathbf{x}) = \frac{1}{2}\left(\nabla\mathbf{v}(\mathbf{x}) + \nabla\mathbf{v}(\mathbf{x})^T\right) \tag{9}$$

By definition, a Newtonian fluid is one for which:

$$\mathbf{T} = -p\mathbf{I} + 2\mu\mathbf{D}, \tag{10}$$

where μ is the absolute viscosity of the fluid[2]. The fluid must satisfy conservation of mass:

$$\nabla \cdot \mathbf{v} = \mathbf{0}, \tag{11}$$

and, conservation of momentum. For a slow moving fluid, conservation of momentum reads:

$$-\mu\Delta\mathbf{v} + \nabla p = \mathbf{b}, \tag{12}$$

[1]It is simple to show that if $\mathbf{S}(\mathbf{I}) = \mathbf{T}(\mathbf{I}) = \mathbf{0}$ and if $\nabla\mathbf{u}$ is small then $\mathbf{S} = \mathbf{T} + o(\nabla\mathbf{u})$ (Cf., e.g. [12, pg. 194-200])

[2]To be precise, this is a definition of a Newtonian fluid which is also independent under change in observer. (Cf., e.g. [12, pg. 147-151])

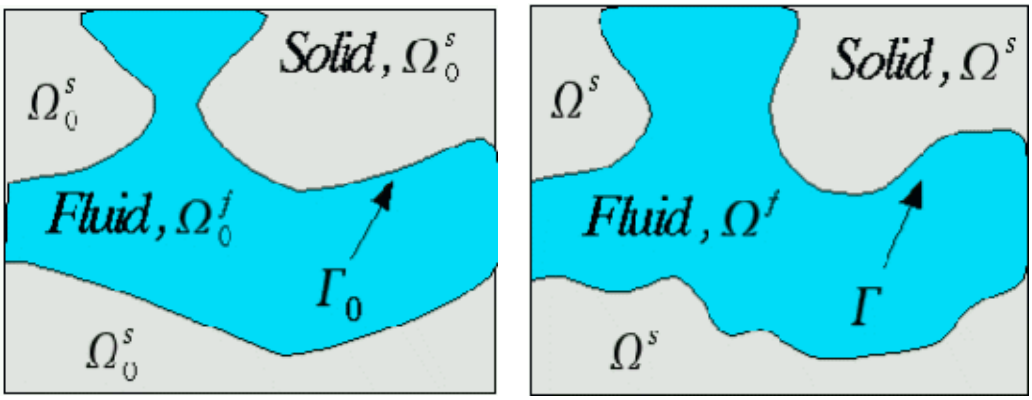

(a) Reference configuration (b) Deformed configuration

FIGURE 1. Schematic of the fluid and structure domains.

where $\mathbf{b}$ is a distributed body force (per unit volume) acting on the fluid.

2.3. **The coupled fluid-structure interaction problem.** Consider now the stationary fluid-structure problem (Figure 1) in the deformed configuration $\Omega = \Omega^f \cup \Omega^s$, where the fluid occupies Ω^f, the solid occupies Ω^s and $\Omega^f \cap \Omega^s = \emptyset$. The part of the boundary shared between the fluid and the solid is denoted by $\Gamma^I = \partial\Omega^f \cap \partial\Omega^s$. We also assume that the deformation $\mathbf{x}(\mathbf{p})$ is such that we don't have contact problems, break-up of the boundary and so on. We have two conditions on the interface. First we need kinematic compatibility, that is, the velocity of the fluid on the interface should be equal to the velocity of the interface itself. This, for a stationary problem, implies that

$$\mathbf{v} = \mathbf{0} \text{ on } \Gamma^I. \tag{13}$$

Further, we also need continuity of tractions, namely (C.f., e.g. [15]):

$$\mathbf{T}^f\mathbf{n} = \mathbf{T}^s\mathbf{n} \quad \text{on } \Gamma^I \tag{14}$$

where $\mathbf{n} = \mathbf{n}^s$ and $\mathbf{n}^s$ is the outward normal to the solid domain. The stress $\mathbf{T}^f$ in the fluid is given by equation (10). Further, we can express the Cauchy stress $\mathbf{T}^s$ in terms of the Piola-Kirchhoff stress using equation (2), which together with Hooke's law (5) implies:

$$-p\mathbf{n} + 2\mu\mathbf{D}\mathbf{n} = \det(\mathbf{F})^{-1}(\mathsf{C} : \mathbf{E})\mathbf{F}^T\mathbf{n} \quad \text{on } \Gamma^I. \tag{15}$$

The FSI problem therefore consists of finding the interface between the two domains, a velocity, pressure and displacements which solve the Stokes (11), (12), and Lamé equations (6) respectively, and also satisfy the interface conditions (13) and (15). More formally, the FSI boundary-value problem is summarized bellow in terms of the unknowns Γ^I, $\mathbf{v}$, p and $\mathbf{u}$: *Find* Γ^I, $\mathbf{v}$, p *and* $\mathbf{u}$ *such that:*

$$\Gamma^I = \left\{\mathbf{p} + \mathbf{u}(\mathbf{p}) | \forall \mathbf{p} \in \Gamma_0^I\right\}, \tag{16}$$

$$\begin{aligned} -\mu\Delta\mathbf{v} + \nabla p &= \mathbf{b} \quad && \text{in } \Omega^f, \\ \nabla \cdot \mathbf{v} &= \mathbf{0} \quad && \text{in } \Omega^f, \\ -\nabla \cdot (\mathsf{C} : \mathbf{E}) &= \mathbf{b}_0 \quad && \text{in } \Omega_0^s, \end{aligned} \tag{17}$$

$$\det(\nabla \mathbf{u} + \mathbf{I})(-p\mathbf{I} + 2\mu \mathbf{D}(\mathbf{x}(\mathbf{p})))\,(\nabla \mathbf{u} + \mathbf{I})^{-T}\,\mathbf{n}_0 = (\mathsf{C} : \mathbf{E})\,\mathbf{n}_0 \ \textit{on}\ \Gamma_0^I, \tag{18}$$

$\mathbf{v}$ *satisfies the kinematic interface condition (13) and in addition* $\mathbf{v}$, p *and* $\mathbf{u}$ *should also satisfy any boundary conditions that might be specified on* $\partial\Omega\backslash\Gamma^I$. Equation (18) is the continuity of tractions (15) expressed on the reference position Γ_0^I of the interface. Observe that the position of the interface is part of the boundary value problem, and the solid-fluid coupling term (18) makes it a nonlinear one.

3. An asymptotic solution for an elastic channel

Consider the steady state laminar flow of incompressible Newtonian fluid through a 2-D channel with elastic walls. The reference geometry of the channel is shown on Figure 2. Denote by L the length of the channel, by l the half of the channel width in the undeformed

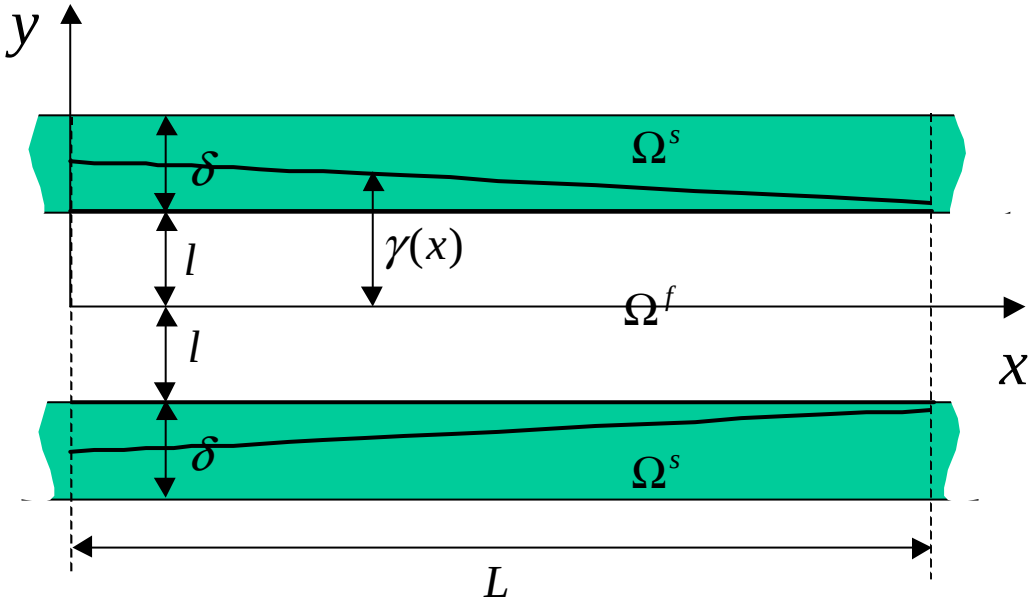

FIGURE 2. Schematic of a section of length L a long elastic channel. The fluid is driven by the pressure gradient.

state, by δ the thickness of the walls in undeformed state. We assume that the channel is long, compared to its height, that is, the parameter ε:

$$\varepsilon = \frac{l}{L} \tag{19}$$

is small. Further we assume that $l \sim \delta$. The fluid is driven by a pressure gradient, and the outer wall of the channel are fixed. We will first normalize the FSI system (16)-(18) for this particular geometry and then we will use a formal expansion of the field variables (pressure, velocity and displacements) with respect to *eps* in order to obtain an asymptotic solution of (16)-(18).

Due to symmetry, we can only consider half of the fluid domain Ω^f and in the undeformed configuration they the fluid and solid occupy

$$\Omega_0^f = \{(x,y), 0 < x < L, 0 < y < l\}, \tag{20}$$

$$\Omega_0^s = \{(x,y), 0 < x < L, l < y < l+\delta\}, \tag{21}$$

respectively. Let us denote the height of the unknown boundary of the fluid-solid interface by $\gamma(x)$.

3.1. **Dimensionless form.** Consider the dimensionless variables:

$$x = L\tilde{x}, \quad y = l\tilde{y}, \quad p(x,y) = \bar{P}\tilde{p}(\tilde{x},\tilde{y}), \tag{22}$$

$$v_1(x,y) = \bar{V}_1\tilde{v}_1(\tilde{x},\tilde{y}), \quad v_2(x,y) = \bar{V}_2\tilde{v}_2(\tilde{x},\tilde{y}), \tag{23}$$

$$u_1(x,y) = \bar{U}_1\tilde{u}_1(\tilde{x},\tilde{y}), \quad u_2(x,y) = \bar{U}_2\tilde{u}_2(\tilde{x},\tilde{y}). \tag{24}$$

In these notations the fluid and solid domain are given by

$$\Omega_f = \{(\tilde{x},\tilde{y}) : 0 < \tilde{x} < 1, \quad 0 < \tilde{y} < \tilde{\gamma}(\tilde{x}))\},$$

$$\Omega_s = \left\{(\tilde{x},\tilde{y}) : 0 < \tilde{x} < 1, \quad \tilde{\gamma}(\tilde{x}) < \tilde{y} < 1 + \frac{\delta}{l})\right\},$$

where

$$\tilde{\gamma}(\tilde{x}) = \frac{\gamma(x)}{l}. \tag{25}$$

Further, we also have ($i = 1, 2$):

$$\frac{\partial p}{\partial x} = \frac{\bar{P}}{L}\frac{\partial \tilde{p}}{\partial \tilde{x}}, \qquad \frac{\partial p}{\partial y} = \frac{\bar{P}}{l}\frac{\partial \tilde{p}}{\partial \tilde{x}}, \tag{26}$$

$$\frac{\partial v_i}{\partial x} = \frac{\bar{V}_i}{L}\frac{\partial \tilde{v}_i}{\partial \tilde{x}}, \qquad \frac{\partial v_i}{\partial y} = \frac{\bar{V}_i}{l}\frac{\partial \tilde{v}_i}{\partial \tilde{x}}, \tag{27}$$

$$\frac{\partial u_i}{\partial x} = \frac{\bar{U}_i}{L}\frac{\partial \tilde{u}_i}{\partial \tilde{x}}, \qquad \frac{\partial u_i}{\partial y} = \frac{\bar{U}_i}{l}\frac{\partial \tilde{u}_i}{\partial \tilde{x}}. \tag{28}$$

It is clear that the scaling parameters can not be chosen independently. Below we will discuss the relations between different scaling parameters.

3.1.1. *Dimensionless Stokes equations.* We first rewrite the Stokes system (11), (12) with respect to dimensionless variables. With the help of equations (26) and (27) we get:

$$-\varepsilon^2\frac{\partial^2\tilde{v}_1}{\partial\tilde{x}^2} - \frac{\partial^2\tilde{v}_1}{\partial\tilde{y}^2} + \varepsilon^2\frac{\bar{P}L}{\mu\bar{V}_1}\frac{\partial\tilde{p}}{\partial\tilde{x}} = 0 \tag{29}$$

$$-\left(\varepsilon^2\frac{\partial^2\tilde{v}_2}{\partial\tilde{x}^2} + \frac{\partial^2\tilde{v}_2}{\partial\tilde{y}^2}\right) + \varepsilon\frac{\bar{P}L}{\mu\bar{V}_2}\frac{\partial\tilde{p}}{\partial\tilde{y}} = 0 \tag{30}$$

$$\frac{\partial\tilde{v}_1}{\partial\tilde{x}} + \frac{\bar{V}_2}{\varepsilon\bar{V}_1}\frac{\partial\tilde{v}_2}{\partial\tilde{y}} = 0. \tag{31}$$

In general, velocity components and pressure can not be scaled independently. We choose $\bar{V}_1$ in accordance with maximal velocity of Poiseuille flow in a rigid channel:

$$\bar{V}_1 = 4V_{1,max}l^2. \tag{32}$$

The other two scales, $\bar{V}_2$ and $\bar{P}$ we express by $\bar{V}_1$. In our case, the $x-$ derivative of the pressure is the driving force for the flow, therefore we want to keep it of unit size. Thus, without loss of generality,

$$\frac{\bar{P}L}{\mu\bar{V}_1}\varepsilon^2 = 1, \tag{33}$$

that is,

$$\bar{P} = \frac{\mu\bar{V}_1}{L\varepsilon^2} = \frac{\mu 4V_{1,max}l^2L}{l^2} = 4\mu V_{1,max}L. \tag{34}$$

Further, we want to have strong conservation of mass. Therefore we require

$$\frac{\bar{V}_2}{\varepsilon\bar{V}_1} = 1, \tag{35}$$

which gives us

$$\bar{V}_2 = \varepsilon\bar{V}_1 \tag{36}$$

The Stokes system (29)-(31) can now be rewritten as

$$\begin{aligned} -\varepsilon^2\frac{\partial^2\tilde{v}_1}{\partial\tilde{x}^2} - \frac{\partial^2\tilde{v}_1}{\partial\tilde{y}^2} + \frac{\partial\tilde{p}}{\partial\tilde{x}} &= 0 \\ -\varepsilon^2\frac{\partial^2\tilde{v}_2}{\partial\tilde{x}^2} - \frac{\partial^2\tilde{v}_2}{\partial\tilde{y}^2} + \varepsilon^{-2}\frac{\partial\tilde{p}}{\partial\tilde{y}} &= 0 \\ \frac{\partial\tilde{v}_1}{\partial\tilde{x}} + \frac{\partial\tilde{v}_2}{\partial\tilde{y}} &= 0. \end{aligned} \tag{37}$$

Here we have used the fact that under the assumptions (33) and (35) we have

$$\frac{\bar{P}L}{\mu\bar{V}_2}\varepsilon\frac{\partial\tilde{p}}{\partial\tilde{y}} = \frac{\mu\bar{V}_1}{\varepsilon^2L}\frac{L}{\mu\bar{V}_2}\varepsilon\frac{\partial\tilde{p}}{\partial\tilde{y}} = \frac{\bar{V}_1}{\varepsilon^2\varepsilon\bar{V}_1}\varepsilon\frac{\partial\tilde{p}}{\partial\tilde{y}} = \varepsilon^{-2}\frac{\partial\tilde{p}}{\partial\tilde{y}}$$

Finally, we also need to express the stress tensor $\mathbf{T}^f$ given by (10) in the fluid domain in terms of the non-dimensional variables:

$$\mathbf{T}^f = \frac{\mu\bar{V}_1L}{l^2}\begin{bmatrix} 2\varepsilon^2\frac{\partial\tilde{v}_1}{\partial\tilde{x}} - \tilde{p} & \varepsilon\left(\frac{\partial\tilde{v}_1}{\partial\tilde{y}} + \varepsilon^2\frac{\partial\tilde{v}_2}{\partial\tilde{x}}\right) \\ \varepsilon\left(\frac{\partial\tilde{v}_1}{\partial\tilde{y}} + \varepsilon^3\frac{\partial\tilde{v}_2}{\partial\tilde{x}}\right) & 2\varepsilon^2\frac{\partial\tilde{v}_2}{\partial\tilde{y}} - \tilde{p} \end{bmatrix}$$

3.1.2. *Dimensionless elasticity problem.* Let us now consider the elastic domain. We restrict our attention only yo isotropic solids. For an isotropic material, the elasticity tensor (5) is necessarily expressed in terms of the two Lamé constants, λ_s and μ_s (cf. eg. [17, 12]), so the stress tensor reduces:

$$\mathbf{S} = \lambda_s\mathrm{tr}\,(\mathbf{E})\,\mathbf{I} + 2\mu_s\mathbf{E}. \tag{38}$$

With the help of (28), $\mathbf{S}$ of the last equation can be expressed as in terms of the non-dimensional variables (24) as:

$$\mathbf{S}^s = \begin{bmatrix} (\lambda_s + 2\mu_s)\frac{\bar{U}_1}{L}\frac{\partial\tilde{u}_1}{\partial\tilde{x}} + \lambda_s\frac{\bar{U}_2}{l}\frac{\partial\tilde{u}_2}{\partial\tilde{y}} & \mu_s\left(\frac{\bar{U}_1}{l}\frac{\partial\tilde{u}_1}{\partial\tilde{y}} + \frac{\bar{U}_2}{L}\frac{\partial\tilde{u}_2}{\partial\tilde{x}}\right) \\ \mu_s\left(\frac{\bar{U}_1}{l}\frac{\partial\tilde{u}_1}{\partial\tilde{y}} + \frac{\bar{U}_2}{L}\frac{\partial\tilde{u}_2}{\partial\tilde{x}}\right) & (\lambda_s + 2\mu_s)\frac{\bar{U}_2}{l}\frac{\partial\tilde{u}_2}{\partial\tilde{y}} + \lambda_s\frac{\bar{U}_1}{L}\frac{\partial\tilde{u}_1}{\partial\tilde{x}} \end{bmatrix}$$

Further assume that

$$\bar{U}_2 = \delta,\ \bar{U}_1 = \varepsilon^0\bar{U}_2 = \delta.$$

Using this scaling for the displacements, the stress in the solid become

$$\mathbf{S}^s = \frac{\delta}{l}\begin{bmatrix} (\lambda_s+2\mu_s)\varepsilon\frac{\partial\tilde{u}_1}{\partial\tilde{x}}+\lambda_s\frac{\partial\tilde{u}_2}{\partial\tilde{y}} & \mu_s\frac{\partial\tilde{u}_1}{\partial\tilde{y}}+\mu_s\varepsilon\frac{\partial\tilde{u}_2}{\partial\tilde{x}} \\ \mu_s\frac{\partial\tilde{u}_1}{\partial\tilde{y}}+\mu_s\varepsilon\frac{\partial\tilde{u}_2}{\partial\tilde{x}} & (\lambda_s+2\mu_s)\frac{\partial\tilde{u}_2}{\partial\tilde{y}}+\lambda_s\varepsilon\frac{\partial\tilde{u}_1}{\partial\tilde{x}} \end{bmatrix}. \tag{39}$$

Further, it is also necessary to write the system of elasticity equations (6) in non-dimensional form. For an isotropic solid, and in the absence of a body force, it is easy to see, the equation (6) reduces to

$$\varepsilon^2\delta(\lambda_s+2\mu_s)\frac{\partial^2\tilde{u}_1}{\partial\tilde{x}^2}+\varepsilon\delta(\lambda_s+\mu_s)\frac{\partial^2\tilde{u}_2}{\partial\tilde{x}\partial\tilde{y}}+\delta\mu_s\frac{\partial^2\tilde{u}_1}{\partial\tilde{y}^2}=0, \tag{40}$$

$$\varepsilon^2\delta\mu_s\frac{\partial^2\tilde{u}_2}{\partial\tilde{x}^2}+\varepsilon\delta(\mu_s+\lambda_s)\frac{\partial^2\tilde{u}_1}{\partial\tilde{x}\partial\tilde{y}}+\delta(\lambda_s+2\mu_s)\frac{\partial^2\tilde{u}_2}{\partial\tilde{y}^2}=0. \tag{41}$$

3.2. **Asymptotic expansion.** Consider now, an asymptotic expansions of the field variables with respect to the small parameter ε:

$$\tilde{v}_i = v_i^0+\varepsilon\tilde{v}_i^1+\varepsilon^2\tilde{v}_i^2+... \tag{42}$$

$$\tilde{p} = \tilde{p}^0+\varepsilon\tilde{p}^1+\varepsilon^2\tilde{p}^2+...$$

$$\tilde{u}_i = \tilde{u}_i^0+\varepsilon\tilde{u}_i^1+\varepsilon^2\tilde{u}_i^2+... \tag{43}$$

3.2.1. *Asymptotic expansion for Stokes system.* Substituting these expansions in Stokes system (37), and collecting terms corresponding to different powers of ε, we get:

ε^{-2} :

$$\frac{\partial\tilde{p}^0}{\partial\tilde{y}}=0. \tag{44}$$

ε^{-1} :

$$\frac{\partial\tilde{p}^1}{\partial\tilde{y}}=0. \tag{45}$$

ε^0 :

$$\begin{aligned} -\frac{\partial^2\tilde{v}_1^0}{\partial\tilde{y}^2}+\frac{\partial^2\tilde{p}^0}{\partial\tilde{x}^2}&=0 \\ -\frac{\partial^2\tilde{v}_2^0}{\partial\tilde{y}^2}+\frac{\partial^2\tilde{p}^2}{\partial\tilde{y}^2}&=0 \\ \frac{\partial\tilde{v}_1^0}{\partial\tilde{x}}+\frac{\partial\tilde{v}_2^0}{\partial\tilde{y}}&=0. \end{aligned} \tag{46}$$

From (44) and (45) we have

$$\tilde{p}^0=\tilde{p}^0(x),\quad \tilde{p}^1=\tilde{p}^1(x). \tag{47}$$

Further, we integrate the first equation from (46) with respect to $\tilde{y}$. The integration limits are from 0 (symmetry line) to $\tilde{y}$. Using the symmetry condition we get

$$-\frac{\partial\tilde{v}_1^0}{\partial\tilde{y}}=-\tilde{y}\frac{\partial\tilde{p}^0}{\partial\tilde{x}}$$

Integrating the last equation with respect to $\tilde{y}$ from $\tilde{y}$ to $\gamma(L\tilde{x})$, we get

$$-\tilde{v}_1^0(\tilde{x},\gamma(L\tilde{x}))+v_1^0(\tilde{x},\tilde{y})=-\frac{1}{2}\left(\gamma^2(L\tilde{x})-\tilde{y}^2\right)\frac{\partial\tilde{p}^0}{\partial\tilde{x}} \tag{48}$$

Using the no-slip boundary condition $\tilde{v}_1^0(\tilde{x},\gamma(L\tilde{x}))=0$, we obtain:

$$\tilde{v}_1^0(\tilde{x},\tilde{y})=-\frac{\gamma^2(L\tilde{x})-\tilde{y}^2}{2}\ \frac{\partial\tilde{p}^0}{\partial\tilde{x}} \tag{49}$$

We will need further the $\tilde{x}-$ derivative of $\tilde{v}_1^0$:

$$\frac{\partial\tilde{v}_1^0}{\partial\tilde{x}}=-\frac{\gamma^2(L\tilde{x})-\tilde{y}^2}{2}\ \frac{\partial^2\tilde{p}^0}{\partial\tilde{x}^2}-L\gamma(L\tilde{x})\frac{\partial\gamma(L\tilde{x})}{\partial\tilde{x}}\frac{\partial\tilde{p}^0}{\partial\tilde{x}} \tag{50}$$

Integrating the continuity equation from 0 to γ and using the boundary conditions $v_1^0(\tilde{x},0)=v_1^0(\gamma)=0$, we get

$$\begin{aligned}0=-\int_0^\gamma\frac{\partial\tilde{v}_1^0(\tilde{x},s)}{\partial\tilde{x}}ds=&-\frac{1}{2}\frac{\partial^2\tilde{p}^0}{\partial\tilde{x}^2}\left(\gamma^3-\frac{\gamma^3}{3}\right)-L\gamma^2(L\tilde{x})\frac{\partial\gamma(L\tilde{x})}{\partial\tilde{x}}\frac{\partial\tilde{p}^0}{\partial\tilde{x}}=\\&-\frac{\partial^2\tilde{p}^0}{\partial\tilde{x}^2}\frac{\gamma^3}{3}-\frac{1}{3}\frac{\partial\gamma^3(L\tilde{x})}{\partial\tilde{x}}\frac{\partial\tilde{p}^0}{\partial\tilde{x}}=-\frac{1}{3}\frac{\partial}{\partial\tilde{x}}\left(\gamma^3(L\tilde{x})\frac{\partial\tilde{p}^0}{\partial\tilde{x}}\right).\end{aligned}$$

That is, we have obtained an equation with respect to $p^0(x)$:

$$\frac{\partial}{\partial\tilde{x}}\left(\gamma^3(L\tilde{x})\frac{\partial\tilde{p}^0}{\partial\tilde{x}}\right)=0. \tag{51}$$

3.2.2. *Expansion for the solid-fluid interface.* So, we obtained equations for $v_1^0,\ v_2^0,\ p^0$, which depend on the unknown free boundary $\gamma(L\tilde{x})$. To get an equation for the free boundary we will use the interface condition for the continuity of the normal component of the stress tensor. So, we need to calculate this normal component. Substituting expansions for velocity and pressure from (42), we obtain

$$\mathbf{T}^f=\frac{\mu\bar{V}_1L}{l^2}\begin{bmatrix}2\varepsilon^2\frac{\partial\tilde{v}_1^0}{\partial\tilde{x}}-p^0-\varepsilon p^1-\varepsilon p^2+O(\varepsilon^3) & \varepsilon\left(\frac{\partial\tilde{v}_1^0}{\partial\tilde{y}}+\varepsilon\frac{\partial\tilde{v}_1^0}{\partial\tilde{y}}+\varepsilon^2\frac{\partial\tilde{v}_2^0}{\partial\tilde{y}}\right)+O(\varepsilon^3)\\ \varepsilon\left(\frac{\partial\tilde{v}_1^0}{\partial\tilde{y}}+\varepsilon\frac{\partial\tilde{v}_1^0}{\partial\tilde{y}}+\varepsilon^2\frac{\partial v_2^0}{\partial\tilde{y}}\right)+O(\varepsilon^3) & 2\varepsilon^2\frac{\partial\tilde{v}_2^0}{\partial\tilde{x}}-p^0-\varepsilon p^1-\varepsilon p^2+O(\varepsilon^3)\end{bmatrix}$$

From this we obtain the zeroth order approximation:
ε^0 :

$$\sigma^{F,0}=\frac{\mu\bar{V}_1L}{l^2}\begin{bmatrix}-\tilde{p}^0 & 0\\ 0 & -\tilde{p}^0\end{bmatrix} \tag{52}$$

The normal vector to the curve $\gamma(x)$ is given by

$$\mathbf{n}=\frac{\mathbf{e}_2-lL\gamma'(L\tilde{x})\mathbf{e}_1}{C_\sigma},\quad\text{where } C_\sigma=\frac{1}{\sqrt{1+L^2\gamma'(L\tilde{x})l^2}}. \tag{53}$$

Using this, we calculate the normal component of the zeroth order term for the stress tensor:

$$\mathbf{T}^{f,0}\mathbf{n}=\frac{1}{C_\sigma}\frac{\mu\bar{V}_1L}{l^2}\left\{\left(\tilde{p}^0lL\gamma'(L\tilde{x})\right)\mathbf{e}_1+-\tilde{p}^0\mathbf{e}_2\right\}. \tag{54}$$

3.2.3. *Asymptotic expansion for elasticity system.* Now we substitute the asymptotic expansion for $u_1,\ u_2$ in the elasticity system (40),(41). From the first elasticity equation (40), at order ε^0, we obtain

$$\mu_s \frac{\partial^2 \tilde{u}_1^0}{\partial \tilde{y}^2} = 0.$$

Integrating with respect to $\tilde{y}$ we get

$$\mu_s \frac{\partial \tilde{u}_1^0}{\partial \tilde{y}} = c_1(\tilde{x}). \tag{55}$$

Integrating from $\tilde{y}$ to $(1+\frac{\delta}{l})$, and using the fact that $\tilde{u}_1^0 = 0$ at the upper boundary, we get

$$\tilde{u}_1^0(\tilde{x},\tilde{y}) = -\frac{\left(1+\frac{\delta}{l}-\tilde{y}\right)}{\mu_s} c_1(\tilde{x}) \tag{56}$$

The second equation (41) from the elasticity system gives, at order ε^0,

$$(\lambda_s + 2\mu_s)\frac{\partial \tilde{u}_2^0}{\partial \tilde{y}} = 0.$$

Integrating with respect to $\tilde{y}$ we get

$$\frac{\partial \tilde{u}_2^0}{\partial \tilde{y}} = \frac{1}{\lambda_s + 2\mu_s} c_2(\tilde{x}) \tag{57}$$

Integrating this equation from $\tilde{y}$ to $(1+\frac{\delta}{l})$, and using the fact that $\tilde{u}_2^0 = 0$ at the upper boundary, we get

$$\tilde{u}_2^0(\tilde{x},\tilde{y}) = -\frac{\left(1+\frac{\delta}{l}-\tilde{y}\right)}{\lambda_s + 2\mu_s} c_2(\tilde{x}) \tag{58}$$

Next, we can substitute the asymptotic expansion (43) for $\tilde{u}_1,\ \tilde{u}_2$ into (39) and obtain the stresses in the solid at order ε^0:

$$\mathbf{S}^{s,0} = \frac{\delta}{l}\begin{bmatrix} \lambda_s \frac{\partial \tilde{u}_2^0}{\partial \tilde{y}} & \mu_s \frac{\partial \tilde{u}_1^0}{\partial \tilde{y}} \\ \mu_s \frac{\partial \tilde{u}_1^0}{\partial \tilde{y}} & (\lambda_s + 2\mu_s)\frac{\partial \tilde{u}_2^0}{\partial \tilde{y}} \end{bmatrix}$$

Finally, we can substitute $\tilde{u}_1^0,\ \tilde{u}_2^0$ as given by (56) and (58) respectively into the last equation and obtain:

$$\mathbf{S}^{s,0} = \frac{\delta}{l}\begin{bmatrix} \frac{\lambda_s}{\lambda_s+2\mu_s} c_2(\tilde{x}) & c_1(\tilde{x}) \\ c_1(\tilde{x}) & c_2(\tilde{x}) \end{bmatrix}.$$

Using this, we calculate the normal component of the zeroth order term for the stress tensor:

$$\mathbf{S}^{s,0}\mathbf{n} = \frac{\delta}{lC_\sigma}\left\{\left(-\frac{\lambda_s}{\lambda_s+2\mu_s}c_2(\tilde{x})lL\gamma'(L\tilde{x}) + c_1(\tilde{x})\right)\mathbf{e}_1 + \left(-c_1(\tilde{x})lL\gamma'(L\tilde{x}) + c_2(\tilde{x})\right)\mathbf{e}_2\right\}. \tag{59}$$

Now using the interface condition for continuity of the normal component of the tensors we get two equations with $c_1(\tilde{x})$ and $c_2(\tilde{x})$ as unknowns:

$$\frac{\delta}{lC_\sigma}\left(c_1(\tilde{x}) - \frac{\lambda_s}{\lambda_s+2\mu_s}c_2(\tilde{x})lL\gamma'(L\tilde{x})\right) = -\frac{\mu\bar{V}_1 L}{l^2 C_\sigma}\tilde{p}^0(\tilde{x})lL\gamma'(L\tilde{x}),$$
$$-\frac{\delta}{lC_\sigma}\left(c_1(\tilde{x})lL\gamma'(L\tilde{x}) - c_2(\tilde{x})\right) = \frac{\mu\bar{V}_1 L}{l^2 C_\sigma}\tilde{p}^0(\tilde{x})$$

Denoting $Q_1 = \frac{\mu\bar{V}_1 L}{l^2} = \bar{P},\ Q_2 = lL\gamma'(L\tilde{x})$ and rearranging terms we obtain:

$$c_1(\tilde{x}) - \frac{\lambda_s}{\lambda_s+2\mu_s}c_2(\tilde{x})Q_2 = Q_1Q_2\tilde{p}^0(\tilde{x}),$$
$$-Q_2c_1(\tilde{x}) + c_2(\tilde{x}) = -Q_1\tilde{p}^0(\tilde{x})$$

From here we obtain

$$c_1(\tilde{x}) = \frac{Q_2\left(-1+\frac{\lambda_s}{\lambda_s+2\mu_s}\right)Q_1}{1-\frac{\lambda_s}{\lambda_s+2\mu_s}Q_2^2}\tilde{p}^0(\tilde{x}) \tag{60}$$

$$c_2(\tilde{x}) = \frac{Q_1 - Q_1Q_2^2}{1-\frac{\lambda_s}{\lambda_s+2\mu_s}Q_2^2}\tilde{p}^0(\tilde{x}) \tag{61}$$

Further, we use the fact that in our case $\gamma' = O(\varepsilon)$ and neglect terms with Q_2^2. Substituting in (56) and (58) we get

$$\tilde{u}_1^0(\tilde{x},\tilde{y}) = -\frac{1+\frac{\delta}{l}-\tilde{y}}{\mu_s}Q_2\left(-1+\frac{\lambda_s}{\lambda_s+2\mu_s}\right)Q_1\tilde{p}^0(\tilde{x}) \tag{62}$$

$$\tilde{u}_2^0(\tilde{x},\tilde{y}) = -\frac{1+\frac{\delta}{l}-\tilde{y}}{\lambda_s+2\mu_s}Q_1\tilde{p}^0(\tilde{x}) \tag{63}$$

Now recall that

$$\tilde{\gamma}(\tilde{x}) = \frac{\gamma(L\tilde{x})}{l} = 1 + \tilde{u}_2(\tilde{x},1),$$

which, together with equation (63), implies

$$\tilde{\gamma}(x) = 1 + \frac{\delta}{l}\frac{1}{\lambda_s+2\mu_s}\bar{P}\tilde{p}^0(\tilde{x}). \tag{64}$$

Equivalently, in dimensional variables,

$$\gamma(x) = l + \frac{\delta}{\lambda_s+2\mu_s}p^0(\tilde{x}). \tag{65}$$

Now we can return to the expression for the $x-$ component of the velocity vector (49). For fixed $\tilde{x}$ (equivalently, x) and a generic function $\tilde{\phi}(\tilde{x},\tilde{y})$ $(= \phi(x,y))$, let us introduce the y-average operator $\langle\cdot\rangle$:

$$\langle\tilde{\phi}(\tilde{x},\tilde{y})\rangle := \frac{1}{2\tilde{\gamma}(\tilde{x})}\int_{-\gamma(\tilde{x})}^{\gamma(\tilde{x})}\tilde{\phi}(\tilde{x},\tilde{y}))dy = \frac{1}{2\gamma(x)}\int_{-\gamma(x)}^{\gamma(x)}\phi(x,y))dy =: \langle\phi(x,y)\rangle. \tag{66}$$

The factor of 2 in the denominator is because we have symmetry of the all field variables with respect of the $x-$ axis and the interval 0 to γ is half of the channel. By averaging

equation (49) we get:

$$\langle \tilde{v}_1(\tilde{x})\rangle = -\frac{1}{3}\gamma^3(L\tilde{x})\langle\frac{\partial \tilde{p}^0}{\partial \tilde{x}}\rangle$$

Substituting here the expression for γ from (65), we obtain

$$\langle \tilde{v}_1(\tilde{x})\rangle = -\frac{1}{3}\left(l + \frac{\delta}{\lambda_s + 2\mu_s}\bar{P}\tilde{p}^0(\tilde{x})\right)^3 \langle\frac{\partial \tilde{p}^0(\tilde{x})}{\partial \tilde{x}}\rangle.$$

Now we can consider the ratio of the mass flux and the pressure gradient which, in the rigid case, gives the permeability K:

$$K := K(\tilde{p}^0(\tilde{x}), \tilde{x}) = -\frac{\langle \tilde{v}_1(\tilde{x})\rangle}{\langle\frac{\partial \tilde{p}^0(\tilde{x})}{\partial \tilde{x}}\rangle} = \frac{1}{3}\left(l + \frac{\delta}{\lambda_s + 2\mu_s}\bar{P}\tilde{p}^0(\tilde{x})\right)^3 \tag{67}$$

Observe, that for a deformable channel, permeability is not a constant, even for fixed fluid and solid materials. We can view it as a function of axial position and averaged pressure. Rewriting the last equation (67) by returning back to dimensional variables, we get:

$$K(p^0(x), x) = \frac{1}{3}\left(l + \frac{\delta}{\lambda_s + 2\mu_s}p^0(\mathbf{x})\right)^3. \tag{68}$$

4. Discretization of the coupled FSI system

In this section we present a numerical method for the solution of the FSI problem. First the continuum problems are recast in weak form in and then, in Section 4.2, are discretized, giving rise to a nonlinear system of algebraic equations. Further, in Section 4.3 an iterative procedure is presented, which solves the coupled FSI problem. It relies on the consecutive solution of solid and fluid subproblems which is discussed in Section 4.4.

4.1. Weak form of the elasticity, Stokes and FSI problems.

Consider a bounded Lipschitz domain Ω and let $(\cdot,\cdot)_\Omega$ be the usual inner product on $L^2(\Omega)$ and, as there is no chance of confusion, also the inner product on $[L^2(\Omega)]^d$, where $d = 2, 3$ is the size of the spatial dimension. Let $H_0^s(\Omega)$, $-1 \le s \le 1$ be the Sobolev spaces and $L_0^2(\Omega)$ be Hilbert space of functions in L^2 having zero mean. For complete development discussion on these subjects, including fractional Sobolev spaces, see [16]. Suppose that both Ω_0^s and Ω^f are Lipschitz domains.

First, in order to simplify notation, it is convenient to introduce the symmetric part of gradient operator:

$$\mathbf{e}(\mathbf{w}) = \frac{1}{2}\left(\nabla\mathbf{w} + (\nabla\mathbf{w})^T\right),$$

for some field $\mathbf{w}$. Observe, that $\mathbf{E} = \mathbf{e}(\mathbf{u})$ and $\mathbf{D} = \mathbf{e}(\mathbf{v})$.

Next, to formulate the elasticity problem, one introduces the bilinear form

$$a_{\Omega_0^s}(\mathbf{u}, \mathbf{w}) = \int_{\Omega_0^s} (\mathsf{C} : \mathbf{e}(\mathbf{u})) : \mathbf{e}(\mathbf{w}) d\mathbf{p}.$$

Let $\hat{\mathbf{u}}_0 \in \left[H^{1/2}(\Gamma_0^D)\right]^d$ be the Dirichlet data given on $\Gamma_0^D \subset \partial\Omega_0^s$, $\hat{s}$ be the Neumann data given on $\Gamma_0^N \subset \partial\Omega_0^s$, and let $\mathbf{b}_0 \in \left[H^{-1}(\Omega^f)\right]^d$ be the distributed body force. The weak form

of the *linear* elasticity problem is: *Find* $\mathbf{u} \in [H^1(\Omega_0^s)]^d$ *such that:*

$$a_{\Omega_0^s}(\mathbf{u}, \mathbf{w}) = (\mathbf{b}_0, \mathbf{w})_{\Omega_0^s} + (\hat{\mathbf{s}}, \mathbf{w})_{\Gamma_0^N}, \qquad \forall \mathbf{w} \in \left[H_D^1(\Omega_0^s)\right]^d, \tag{69}$$

$$\mathbf{u} = \hat{\mathbf{u}}_0, \qquad \text{on } \Gamma_0^D. \tag{70}$$

The first of the above equations is obtained by multiplying equation (6) by a test function and integrating by parts. Note that the Neumann boundary condition appears on the right hand side as the surface integral.

The stability of the weak elasticity problem follows from the classical Korn's inequality: *There exists a positive constant* $C_1 = C_1(\Omega_0^s) > 0$ *independent of* $\mathbf{u}$*, such that:*

$$\int_{\Omega_0^s} \mathbf{e}(\mathbf{u}) : \mathbf{e}(\mathbf{u}) d\mathbf{p} \geq C_1 ||\mathbf{u}||^2_{1,\Omega_0^s} \quad \forall \mathbf{u} \in \left[H_D^1(\Omega_0^s)\right]^d. \tag{71}$$

The conditions for its validity and a proof of this nontrivial inequality can be found, for example, in [19, 9]. It will be assumed here that the elasticity tensor C and boundary conditions (7) and (8) are such that (71) is satisfied. This is a standard subject which will not be discussed further, the reader is instead referred to [19].

In the case of the Stokes problem assume, again for simplicity, that homogeneous Dirichlet boundary data is given and let $\mathbf{b} \in \left[H^{-1}(\Omega^f)\right]^d$. The weak form of the Stokes equation is: *Find* $\mathbf{v} \in \left[H_0^1(\Omega^f)\right]^d$, $p \in L_0^2(\Omega^f)$ *such that:*

$$\begin{array}{ll} D_{\Omega^f}(\mathbf{v}, \mathbf{w}) - (p, \nabla \cdot \mathbf{w})_{\Omega^f} = (\mathbf{b}, \mathbf{w})_{\Omega^f}, & \forall \mathbf{w} \in \left[H_0^1(\Omega^f)\right]^d, \\ -(\nabla \cdot \mathbf{v}, q)_{\Omega^f} = 0, & \forall q \in L_0^2. \end{array} \tag{72}$$

Here $D_{\Omega^f}(\mathbf{v}, \mathbf{w})$ is the vector Dirichlet form

$$D_{\Omega^f}(\mathbf{v}, \mathbf{w}) = \int_{\Omega^f} \mu \nabla \mathbf{v} : \nabla \mathbf{w} d\mathbf{x}.$$

The existence and uniqueness of solution to the Stokes problem follows from the classical inf-sup condition[3] (cf., e.g., [9]): *There exists a positive constant* $C_2 = C_2(\Omega^f) > 0$*, independent of* $\mathbf{v}$ *and* p*, and such that:*

$$\inf_{\forall p \in L_0^2(\Omega^f)} \sup_{\forall \mathbf{v} \in \left[H_0^1(\Omega^f)\right]^d} \frac{(p, \nabla \cdot \mathbf{v})^2_{\Omega^f}}{D_{\Omega^f}(\mathbf{v}, \mathbf{v}) ||p||^2} > C_2. \tag{73}$$

For a complete discussion of the weak problem (72) and condition (73) the reader is referred to the classical text [9].

To write a weak form of the FSI problem, observe that the interface condition (18) can be treated as a nonlinear Neumann boundary condition for the solid problem only. Accordingly, we introduce the nonlinear form:

$$g_{\Gamma_0^I}(\mathbf{v}, \mathbf{u}, p, \mathbf{w}) = \int_{\Gamma_0^I} \left\{ \det(\nabla \mathbf{u} + \mathbf{I})(-p\mathbf{I} + 2\mu \mathbf{e}(\mathbf{v})) \left(\nabla \mathbf{u} + \mathbf{I}\right)^{-T} \mathbf{n}_0 \right\} \cdot \mathbf{w} ds. \tag{74}$$

After integrating by parts the balance of linear momentum for the solid and fluid, it is trivial to check that the boundary value problem (17)-(18) can be restated in the following

[3]The inf-sup condition is also referred to by the name Ladyzenskaya-Babuska-Brezzi (LBB) condition.

weak form: *Find the interface* Γ^I*, the deformed configuration of the fluid domain* Ω^f*, the displacements* $\mathbf{u} \in [H^1(\Omega_0^s)]^d$*, velocity* $\mathbf{v} \in \left[H_0^1(\Omega^f)\right]^d$ *and pressure* $p \in L_0^2(\Omega^f)$ *such that:*

$$
\begin{aligned}
D_{\Omega^f}(\mathbf{v},\mathbf{w}) - (p, \nabla\cdot\mathbf{w})_{\Omega^f} &= (\mathbf{b},\mathbf{w})_{\Omega^f}, && \forall \mathbf{w} \in \left[H_0^1(\Omega^f)\right]^d, \\
-(\nabla\cdot\mathbf{v}, q)_{\Omega^f} &= 0, && \forall q \in L_0^2, \\
a_{\Omega_0^s}(\mathbf{u},\mathbf{w}) &= (\mathbf{b}_0,\mathbf{w})_{\Omega_0^s} + g_{\Gamma_0^I}(\mathbf{v},\mathbf{u},p,\mathbf{w}), && \forall \mathbf{w} \in [H_D^1(\Omega_0^s)]^d, \\
\Gamma &= \{\mathbf{p} + \mathbf{u}(\mathbf{p}) | \forall \mathbf{p} \in \Gamma_0\}\,.
\end{aligned}
\tag{75}
$$

In addition $\mathbf{v}$*,* p *and* $\mathbf{u}$ *should also satisfy the appropriate boundary conditions specified on* $\partial\Omega\backslash\Gamma^I$*.*

4.2. **Discretization of the field variables.** Let $U_{\mathbf{u}}$, $U_{\mathbf{v}}$ and U_p be finite-dimensional subspaces for the displacements, velocity and pressure respectively. Then the first three equations in (75) lead to the following nonlinear system of algebraic equations:

$$
\begin{pmatrix} \mathbf{A}(\mathbf{u}) & \mathbf{C}^T(\mathbf{u}) & \mathbf{0} \\ \mathbf{C}(\mathbf{u}) & \mathbf{0} & \mathbf{0} \\ \mathbf{0} & \mathbf{0} & \mathbf{K} \end{pmatrix} \begin{pmatrix} \mathbf{v} \\ \mathbf{p} \\ \mathbf{u} \end{pmatrix} = \begin{pmatrix} \mathbf{b}_f(\mathbf{u}) \\ \mathbf{d} \\ \mathbf{b}_s + \mathbf{g}(\mathbf{u},\mathbf{v},\mathbf{p}) \end{pmatrix},
\tag{76}
$$

where the blocks $\mathbf{A}(\mathbf{u})$ and $\mathbf{K}$ correspond to the bilinear forms $D_{\Omega^f}(\cdot,\cdot)$ and $a_{\Omega_0^s}(\cdot,\cdot)$, while the blocks $\mathbf{C}(\mathbf{u})$ and $\mathbf{C}(\mathbf{u})^T$ couple the velocity and pressure unknowns. Since the position of Γ^I and hence Ω^f depends on $\mathbf{u}$, both $\mathbf{A}$ and $\mathbf{C}$ are functions of the displacement. The vector-columns $\mathbf{b}_f(\mathbf{u})$ and $\mathbf{b}_s$ correspond to the body force in the fluid and solid respectively, modified by application of essential (Dirichlet, periodic, etc.) boundary conditions. Note that the vector $\mathbf{d}$ appears in the right-hand side of (76) when the essential boundary conditions are applied by matrix transformations. If, for example, they are applied by a penalty method, then $\mathbf{d} \equiv \mathbf{0}$.

It is important to observe that the coupling between the fluid and the structure (15) appears on the right hand side of (76) as the nonlinear vector-function $\mathbf{g}(\mathbf{u},\mathbf{v},\mathbf{p})$ which corresponds to the form $g_{\Gamma_0^I}(\cdot,\cdot,\cdot,\cdot)$. Note that the fluid tractions on acting on the solid are evaluated in the reference configuration, i.e. on Γ_0^I.

4.3. **Dirichlet-Neumann iterative scheme.** One way to solve the BVP (17), (16) is to use an iterative scheme which successively solves separate problem on the two domains. Considering the following approach:

- Solve the Stokes equation in the fluid domain treating the solid as a rigid body;
- Transfer the forces to the solid;
- Calculate the displacement field in the solid and then update the fluid domain.

The second step needs some further clarification. In order to solve an elasticity problem the boundary conditions should be specified on the reference configuration, while the tractions computed from a fluid solution are given in the deformed configuration. For given velocities and pressure, the interface condition (15) specifies the traction on the solid domain in the deformed configuration, so we have to use the definition (2) of the Piola-Kirchhoff stress tensor and convert the tractions to the reference configuration. That is exactly what happens when $g(\cdots)$ is evaluated. It is not difficult to check that the above algorithm corresponds to a fixed point iteration using the following linearization of (76): *Set* $\mathbf{u}_0 = \mathbf{0}$*,* $\mathbf{v}_0 = \mathbf{0}$*,* $\mathbf{p}_0 = 0$*;*

given $(\mathbf{u}_k, \mathbf{v}_k, p_k)^T$, *find* $(\mathbf{u}_{k+1}, \mathbf{v}_{k+1}, p_{k+1})^T$ *such that:*

$$\begin{pmatrix} \mathbf{A}(\mathbf{u}_k) & \mathbf{C}^T(\mathbf{u}_k) & \mathbf{0} \\ \mathbf{C}(\mathbf{u}_k) & \mathbf{0} & \mathbf{0} \\ \mathbf{0} & \mathbf{0} & \mathbf{K} \end{pmatrix} \begin{pmatrix} \mathbf{v}_{k+1} \\ \mathbf{p}_{k+1} \\ \mathbf{u}_{k+1} \end{pmatrix} = \begin{pmatrix} \mathbf{b}_f(\mathbf{u}_k) \\ \mathbf{d} \\ \mathbf{b}_s + \mathbf{g}(\mathbf{u}_k, \mathbf{v}_{k+1}, \mathbf{p}_{k+1}) \end{pmatrix}. \tag{77}$$

Since the matrix on the left-hand side of the above equation is block-diagonal the block corresponding to the fluid is solved first:

$$\begin{pmatrix} \mathbf{v}_{k+1} \\ \mathbf{p}_{k+1} \end{pmatrix} = \begin{pmatrix} \mathbf{A}(\mathbf{u}_k) & \mathbf{C}^T(\mathbf{u}_k) \\ \mathbf{C}(\mathbf{u}_k) & \mathbf{0} \end{pmatrix}^{-1} \begin{pmatrix} \mathbf{b}_f(\mathbf{u}_k) \\ \mathbf{d} \end{pmatrix}. \tag{78}$$

Once $\mathbf{v}_{k+1}$ and $\mathbf{p}_{k+1}$ are available, the block corresponding to the solid, i.e.,

$$\mathbf{u}_{k+1} = \mathbf{K}^{-1} \left(\mathbf{b}_s + \mathbf{g}(\mathbf{u}_k, \mathbf{v}_{k+1}, \mathbf{p}_{k+1}) \right) \tag{79}$$

is solved. This iterative scheme can be expresses more explicitly in the following

Algorithm 4.3.1. *(Dirichlet-Neumann domain decomposition method for the FSI problem) Set* $\mathbf{u}_0 = \mathbf{0}$. *For* $k = 0, 1, ...$ *until convergence do:*

1. *Find* $\mathbf{v}_k, p_k$ *which satisfy the Stokes equations (11),(12) in* Ω_k^f *with the no-slip boundary condition on the interface* Γ_k^I *and the appropriate boundary conditions on* $\partial\Omega_k^f \backslash \Gamma_k^I$.
2. *Compute the traction* $\mathbf{t}_k = \mathbf{T}\mathbf{n}_k$ *on the interface* Γ_k^I *using equation (15).*
3. *Based on* $\mathbf{t}_k$ *compute the tractions* $\mathbf{s}_k$ *in the reference configuration of the interface, i.e.* Γ_0^I *using equation (2) and the current iterate for the displacements* $\mathbf{u}_k$.
4. *Find* $\mathbf{u}_{k+1}$ *which satisfies the balance of linear momentum (6) in* Ω_k^s *with* $\mathbf{S}\mathbf{n}_0 = \mathbf{s}_k$ *and the appropriate boundary data on* $\partial\Omega_0^s \backslash \Gamma_0^I$.
5. *Compute* $\Gamma_{k+1}^I = \left\{ \mathbf{p} + \mathbf{u}_{k+1}(\mathbf{p}) | \forall p \in \Gamma_0^I \right\}$ *and* Ω_{k+1}^f*:*
6. *Check convergence:* $||\mathbf{u}_{k+1} - \mathbf{u}_k||_{\Gamma_{k+1}^I} < TOLERANCE * ||\mathbf{u}_{k+1}||_{\Gamma_{k+1}^I}$. *The norm is the discrete euclidian norm of the interface nodal values.*

It is clear that if the interface converges to a fixed position we will have a velocity and pressure field which satisfy the Stokes equation (11),(12), a displacement field which satisfies the elasticity equations (6), and as a results of the converged interface, the interface condition (15) will also be satisfied.

4.4. **FEM approximation of the FSI problem.** In this section the FEM approximation for the FSI problem is introduced. Both the solid and fluid problems are discretized using the FEM method. The elasticity problem is solved by standard linear triangular elements. That is, given a triangulation $\mathcal{T}_h^s$ of Ω_0^s, the approximation space for the displacements is chosen to be:

$$U_{\mathbf{u}} = \left[\left\{ u \in C^0(\Omega_0^s) | u \text{ is linear on } \forall \tau \in \mathcal{T}_h^s \right\} \right]^d \subset \left[H^1(\Omega_0^s) \right]^d. \tag{80}$$

The Stokes problem is solved using the P_2P_1 (Taylor-Hood) element pair. Given a triangulation $\mathcal{T}_h^f$ of Ω^f the approximation spaces for the velocity and pressure are defined by

$$U_{\mathbf{v}} = \left[\left\{ v \in C^0(\Omega^f) | v \text{ is quadratic polynomial on } \forall \tau \in \mathcal{T}_h^f \right\} \right]^d \subset \left[H^1(\Omega^f) \right]^d \tag{81}$$

$$U_p = \left\{ p \in C^0(\Omega^f) | p \text{ is linear on } \forall \tau \in \mathcal{T}_h \right\} \subset H^1(\Omega^f) \subset L^2(\Omega^f) \tag{82}$$

respectively.

It follows from the inclusion $U_{\mathbf{u}} \subset [H^1(\Omega_0^s)]^d$ that Korn's inequality (71) is satisfied on the subspace $U_{\mathbf{u}}$, therefore the discretized elasticity problem has a unique solution. The selection of the approximation spaces for the Stokes problems is governed by the fact that they must satisfy the discrete version of the inf-sup, that is,

$$\inf_{\forall p \in U_p} \sup_{\forall \mathbf{v} \in U_{\mathbf{v}}} \frac{(p, \nabla \cdot \mathbf{v})^2_{\Omega^f}}{D_{\Omega^f}(\mathbf{v}, \mathbf{v}) ||p||^2_{\Omega^f}} > C_2 \tag{83}$$

in order to have a stable approximation. Such elements are said to be LBB stable. While many other elements are known to be LBB stable [11], the Taylor-Hood element was chosen because it provides a balanced approximation for both velocity and pressure [2].

The two discretized domains have piecewise straight boundaries so the use of linear approximation for the displacement field simplifies things because Γ_k^I will remain piecewise straight and the two meshes will be point-wise conforming at all times. The interface condition (13) however is enforced only weakly, because the stresses in the solid are piecewise constants while the stresses in the fluid are piecewise linear functions[4]. Note that both are discontinuous across elements. Investigation of curvilinear interface boundaries and/or higher order approximation spaces for the elasticity problem was outside the scope if this work.

4.5. **Solution methods for the solid and fluid subproblems.** In this section the methods used to solve the linear systems of algebraic equations (77) arising in the discretization (75), (80) - (82) of the previous section are discussed. Some other practical issues of the implementation of Algorithm 4.3.1 such as mesh regeneration are also described.

In general, the block matrices appearing in (77) are large sparse matrices so they can be stored efficiently in machine memory, however inverting them explicitly is both computationally expensive and the resulting matrices are dense. Therefore, at each iterations of Algorithm 4.3.1 instead of computing and applying directly the inverse matrices in (78) and (79) one solves the equivalent linear systems by an iterative method. Since these two systems have to be solved once per each iteration of Algorithm 4.3.1, it is important that this is done so efficiently. The methodology used to solve these two linear systems is described next.

4.5.1. *Linearized elasticity problem.* The linear system corresponding to equation (79) is

$$\mathbf{K}\mathbf{u}_{k+1} = \mathbf{b}_s + \mathbf{g}(\mathbf{u}_k, \mathbf{v}_{k+1}, \mathbf{p}_{k+1}). \tag{84}$$

The stiffness matrix $\mathbf{K}$ is symmetric, positive definite and sparse, making it ideal for the application of the Preconditioned Conjugate Gradient (PCG) method (the two classical references are [13, 14], see also [10, 20]).

The preconditioner used in this work is based upon a block diagonal factorization of the stiffness matrix. Denote by $\phi_i^{(j)}$, $i = 1, ..., d$, $j = 1, ..., N_u$, the nodal basis functions for the displacement space $U_{\mathbf{u}}$. If the nodal unknowns are ordered by displacement component, i.e. the vector column $\mathbf{u} = (u_1^{(1)}, u_1^{(2)}, ..., u_1^{(N_u)}, u_2^{(1)}, ...)^T$ contains all the nodal unknowns of the first displacement component, followed by all the unknowns for the second one, and so on,

[4]Since the contributions to the stresses in the fluid come both from the pressure and the velocity gradients things will not change if one uses other approximations for the fluid, e.g. P_2P_0.

then the stiffness matrix $\mathbf{K}$ has the following block structure:

$$\mathbf{K} = \begin{pmatrix} \mathbf{K}_{11} & \cdots & \mathbf{K}_{1d} \\ \vdots & \ddots & \vdots \\ \mathbf{K}_{d1} & \cdots & \mathbf{K}_{dd} \end{pmatrix}. \tag{85}$$

This ordering allows for a robust preconditioning of the linear system. Consider the matrix $\mathbf{K}_{SDC} = diag(\mathbf{K}_{11}, \ldots, \mathbf{K}_{dd})$ which contains only the diagonal blocks of $\mathbf{K}$. It can be shown [7] that $\mathbf{K}_{SDC}$ is an optimal preconditioner[5] for $\mathbf{K}$, that is, the condition number κ of the preconditioned matrix satisfies

$$\kappa\left((\mathbf{K}_{SDC})^{-1}\mathbf{K}\right) \leq \frac{d-1}{C_1}\frac{1-\nu}{1-2\nu}. \tag{86}$$

where C_1 is the mesh independent constant, appearing in (71) and ν is Poisson ratio. For proof and improvements in the above estimate, see [7, 19]. In general the application of $(\mathbf{K}_{SDC})^{-1}$ at each CG iteration for (84) can be done by multigrid in linear time, leading to an optimal method. A different (and simpler) approach, selected here, is to use a $MIC(0)$ factorization of $\mathbf{K}_{SDC}$ which results in condition number of order $\mathcal{O}\left(h^{-1}\right)$. As a result, the CG finds a solution in $\mathcal{O}\left(h^{-1/2}\right)$ iterations and the overall algorithm complexity is $\mathcal{O}\left(N_u^{1+\frac{1}{2d}}\right)$. For detailed description of the $MIC(0)$ preconditioner see [7]. For the problems under consideration this preconditioner proved to be adequate enough.

4.5.2. *Stokes problem.* Solving the linear system of algebraic equations for the Stokes problem is an active area of research and there is no general agreement on what is the most efficient way [8, 22, 2]. In this work, the fluid problem (78) is solved again by the PCG method, but applied to the Schur complement for the pressure variables. A comprehensive study of pressure Schur complement methods can be found in [22]. For notational simplicity, in this section the implicit dependence on $\mathbf{u}_k$ of the matrices $\mathbf{A}$ and $\mathbf{C}$ will be suppressed.

The Stokes system corresponding to equation (78)

$$\begin{pmatrix} \mathbf{A} & \mathbf{C}^T \\ \mathbf{C} & \mathbf{0} \end{pmatrix} \begin{pmatrix} \mathbf{v} \\ \mathbf{p} \end{pmatrix} = \begin{pmatrix} \mathbf{b}_f \\ \mathbf{d} \end{pmatrix} \tag{87}$$

is indefinite, which makes impossible direct application of the CG. While generalized Krylov subspace methods such as MINRES [10, 20] can still be used, preconditioning is not an obvious task. Therefore the Schur complement method for the pressure variable is used [8, 2]. Observe that $\mathbf{A}$ is an invertible matrix, so one can eliminate the first row of (87) to obtain

$$\mathbf{S}\mathbf{p} = \mathbf{C}\mathbf{A}^{-1}\mathbf{b}_f - \mathbf{d}. \tag{88}$$

where $\mathbf{S}$ is the Schur complement matrix[6]:

$$\mathbf{S} = \mathbf{C}\mathbf{A}^{-1}\mathbf{C}^T.$$

[5] In the sense that it is independent of the mesh parameter h.

[6] The notation for the Schur complement is unique to this section alone, therefore there is no chance of confusion with the Piola-Kirchhoff stress.

The invertibility of $\mathbf{S}$, which is also a symmetric matrix, follows from the inf-sup condition. To see this, take an arbitrary element $\mathbf{q} \in U_p$ of the discrete pressure space and observe that:

$$\left(\mathbf{C}\mathbf{A}^{-1}\mathbf{C}^T\mathbf{q}, \mathbf{q}\right) = \sup_{w \in U_{\mathbf{v}}} \frac{(\mathbf{q}, \mathbf{C}\mathbf{w})^2}{(\mathbf{A}\mathbf{w}, \mathbf{w})}$$

It follows from (83) that the right-hand side of the last equation satisfies

$$\sup_{w \in U_{\mathbf{v}}} \frac{(\mathbf{q}, \mathbf{C}\mathbf{w})^2}{(\mathbf{A}\mathbf{w}, \mathbf{w})} \geq C_2 ||\mathbf{w}||^2, \quad \forall \mathbf{q} \in U_p,$$

therefore $\mathbf{S}$ is a positive definite matrix, and hence invertible. Secondly, since it is symmetric, the CG method can be applied to the reduced system (88). Now, in general, $\mathbf{S}$ is a dense matrix and it is expensive to evaluate it explicitly. However, the CG algorithm only requires the computation of the action of $\mathbf{S}$ on a vector, and this can be done, provided that one can solve linear systems with $\mathbf{A}$ efficiently.

To see how the last can be done, denote again by $\phi_i^{(j)}$, $i = 1, ..., d$, $j = 1, ..., N_v$, the nodal basis functions of the velocity space $U_{\mathbf{v}}$ and by $\psi^{(j)}$, $j = 1...N_p$ the nodal basis of pressure space U_p. Upon ordering the velocity unknowns by component, the block $\mathbf{A}$ has a block-diagonal structure:

$$\mathbf{A} = diag\left(\mathbf{A}_1, ..., \mathbf{A}_d\right),$$

where the components of each block $\mathbf{A}_l$ are given by (no implicit summation by repeated indices assumed!):

$$(A_l)_{ij} = \mu \int_{\Omega^f} \sum_{k=1}^{d} \phi_{l,k}^{(i)} \phi_{l,k}^{(j)} d\mathbf{x}, \quad l = 1, ..., d. \tag{89}$$

Similarly, $\mathbf{C} = (\mathbf{C}_1, ..., \mathbf{C}_d)$, where (no implicit summation):

$$(C_l)_{ij} = -\int_{\Omega^f} \phi_{l,l}^{(i)} \psi^{(j)} d\mathbf{x}, \quad l = 1, ..., d. \tag{90}$$

Since $\mathbf{A}$ is block-diagonal, inverting it reduces to inverting each block. Observe, however, that each block $\mathbf{A}_l$ corresponds to a Laplacian stiffness matrix, and these can be inverted efficiently (in $\mathcal{O}(1)$ CG iterations with a multigrid preconditioner, for example). That is, when the action of $(\mathbf{A}_l)^{-1}$ is required, one solves the corresponding linear system for $\mathbf{A}_l$ using the CG with an appropriate preconditioner. In the current work, a threshold ILU factorization [20] proved to be sufficient for the problems under consideration.

Returning back to the reduced linear system for the Schur complement (88), the condition number of $\mathbf{S}$ is independent of the mesh parameter h, although it depends on the geometry of the domain Ω^f [22]. It is nevertheless desirable to precondition it. As a preconditioner for $\mathbf{S}$ one can use a mass matrix $\mathbf{M}^p$ on the pressure space:

$$M^p{}_{ij} = \int_{\Omega^f} \psi^{(i)} \psi^{(j)} d\mathbf{x}, \tag{91}$$

which, as shown in [22], reduces the total number of iterations several times. In the current work, $\mathbf{M}^p$ is the selected preconditioner for $\mathbf{S}$ and the blocks $\mathbf{A}_l$ are preconditioned with a threshold ILU factorization [20]. As a final remark, $\mathbf{M}^p$ is a mass matrix, therefore the application of $(\mathbf{M}^p)^{-1}$ (by CG iteration) requires $\mathcal{O}(1)$ CG iterations.

To summarize, the fluid problem is solved by applying the CG to the reduced system (88). At each CG iteration, the application of $\mathbf{A}^{-1}$ in the matrix-vector multiplication with

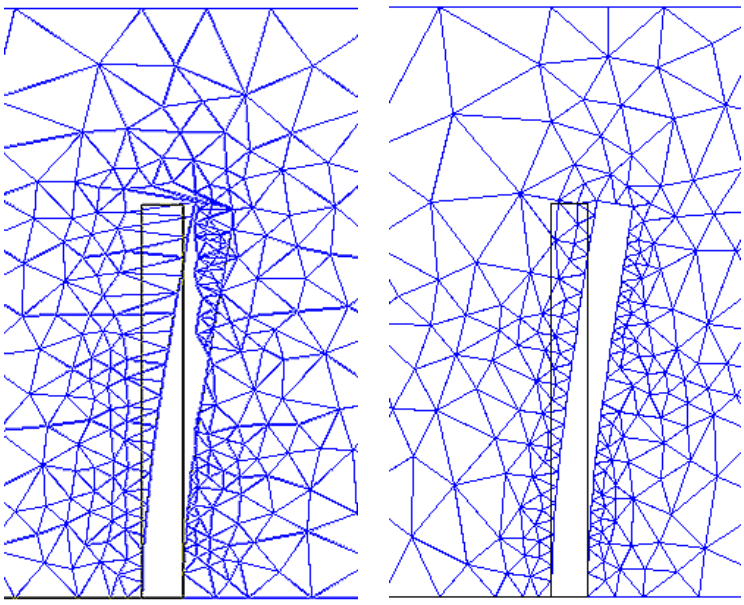

(a) Degenerated mesh (b) Regenerated mesh

FIGURE 3. A 2D degenerate mesh. In this example an elastic obstacle deforms to the left in response to flow in the channel. The solid lines indicate its initial configuration. If only the boundary nodes of the fluid mesh are moved, it degenerates (left). The second mesh (right) is obtained after remeshing the fluid domain.

$\mathbf{S}$ is performed by an internal CG iteration with an ILU preconditioner for $\mathbf{A}$. Also, the application of the preconditioner $(\mathbf{M}^p)^{-1}$ for the Schur complement $\mathbf{S}$ is performed again by an internal CG iteration.

4.5.3. *Fluid mesh regeneration.* At the beginning of Algorithm 4.3.1 one has a conforming triangulation of both the solid and fluid domains. At the end of each iteration (step 5) the fluid domain is updated and as a result, the mesh also has to change. On the other hand, the elasticity equation is always solved in the original configuration, so the elastic mesh remains unchanged. Since only conforming meshed are considered, the modification of the fluid mesh must be such that conformity is maintained on Γ^I. That is, when the interface is deformed using the computed displacement $\mathbf{u}_{k+1}$, solid vertices will coincide with fluid vertices and solid segments (faces in 3D) should coincide with fluid ones.

The easiest approach is to move the interface vertices at the end of step 5 of Algorithm 4.3.1 which will affect only the elements which contain them. This will work as long as the interface displacements are small compared to the local mesh size. If the mesh size near the interface is comparable to the displacements of the interface the mesh can loose quality or completely degenerate if a vertex is moved into another element (Figures 3 and 4). As a result, given the domain and boundary condition, the mesh size in the fluid domain cannot be too small. Such a restriction is clearly unacceptable. It can be overcome by either globally modifying

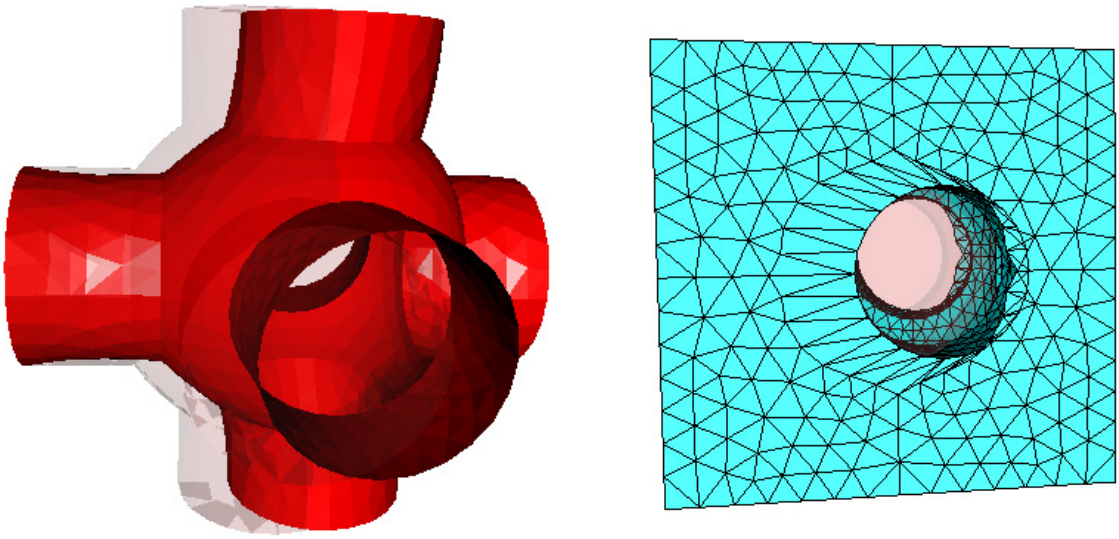

(a) Flow external to a elastic skeleton (b) Degenerated mesh after first iteration

FIGURE 4. A 3D degenerate mesh. Another case when the mesh degenerates after a new position of the interface is computed. Shown are the initial (transparent shade) and final position (solid red) of the interface Γ^I (a) and the degenerated mesh after the first iteration (b). The domain is the unit cube and the solid geometry is formed by the intersection of three perpendicular cylinders and a central circle. The flow is from left to right, is exterior to the solid (the caps on the cylinders are not shown) and the boundary conditions allow the caps of the two cylinders perpendicular to the flow direction to slide on the side of the unit cube. Unlike the 2D case, the regeneration of the mesh involves both the interior and part of the surface mesh.

the existing mesh, for example, by solving an artificial elasticity problem in the fluid domain or by remeshing it (locally or globally).

The global remeshing approach is selected here because of the ready availability of mesh generators which could do that. At the conclusion of step 5, the elements with vertices on the interface are modified and if the resulting mesh has poor quality and/or it degenerates then the entire fluid domain is remeshed, retaining the same boundary segments in 2D and the same interface faces in 3D. Note that in 3D, in addition to the entire volume mesh, one also has to modify part of the surface mesh as can be seen from figure Figure 4, while keeping the interface conforming. In principle local regeneration of the mesh (after removing low quality/degenerate elements) is an interesting possibility which can significantly speed up the process, however developing the software necessary to utilize this strategy was outside of the scope of this research.

5. Numerical Examples

Three model problems were considered in order to test the Dirichlet-Neumann iterative scheme of Section 4.3. The first two model problems involve flow in the elastic channel

geometry of Section 3, while the third one is for a channel with elastic segment. The first model problem is used to demonstrate the convergence properties of the iterative scheme with regard to various problem parameters. The second problem is set up in the same type of geometry, but with slightly different boundary conditions, so that a comparison can be made between the numerical solutions and the asymptotic solution of Section 3. The last problem of flow in a channel with an elastic segment demonstrates the highly nonlinear dependence of permeability on the pressure gradient across the channel.

5.1. **Flow through an elastic channel.** The first model problem to be considered is one for a flow through an elastic channel. The geometry is shown on Figure 5. The channel has length 5 and thickness 1. The thickness of each of the elastic slabs is 0.2. The material parameters used for the solid are $E = 1.44$ and $\nu = 0.2$ while the fluid has viscosity $\mu = 0.1$ and density $\rho = 1$. The velocity distribution at the inlet is that of a developed Poiseuille flow: $v_x = 4 * V_{max} y(1-y)$, where the constant V_{max} is the maximal inflow velocity (achieved at $y = 0.5$).

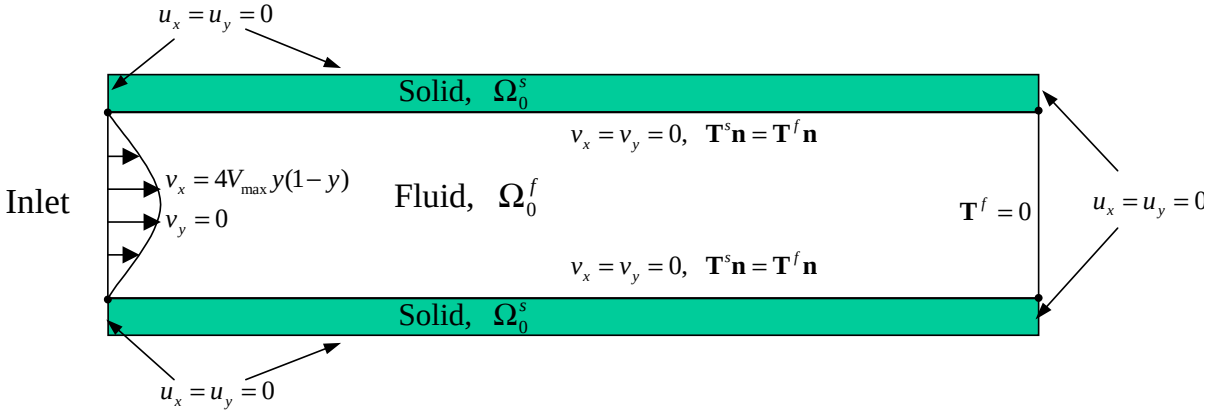

FIGURE 5. Model problem geometry

First the numerical algorithm is tested for $V_{max} = 1/4$ and a (triangular) mesh with $h \sim 16 * 10^{-2}$ in the fluid domain and $h \sim 4 * 10^{-2}$ in the solid domain. No triangle had internal angles less than 30 degrees. The mesh is chosen coarser in the fluid domain because of the 2-nd order accuracy for the velocity (and 1-st order for the pressure/stress) compared to the 1-st order approximation in the solid region. The computed pressure and velocity profiles are displayed on Figures 6(a) and 6(b).

Next, the problem is solved for several values of V_{max} and three different mesh sizes. This is done in order to get a preliminary idea of convergence rate sensitivity of the iterative scheme of Algorithm 4.3.1 to the inflow velocity and mesh size. The number of iterations it took to reach relative precision 10^{-6} is reported in Table 1. Also given in the table is the maximum vertical displacement in the solid. Based on the non-dimensional analysis of Section 3 for this problem varying input velocity V_{max} is the same as varying the elastic stiffness E or fluid viscosity μ.

It can be concluded from this table that the iteration numbers depend on the inlet velocity which in turn directly affects the magnitude of the interface displacement. In general, numerical experiments suggest that the important parameter is the magnitude of the interface displacements. On the other hand the iteration convergence rate seem not to depend on the

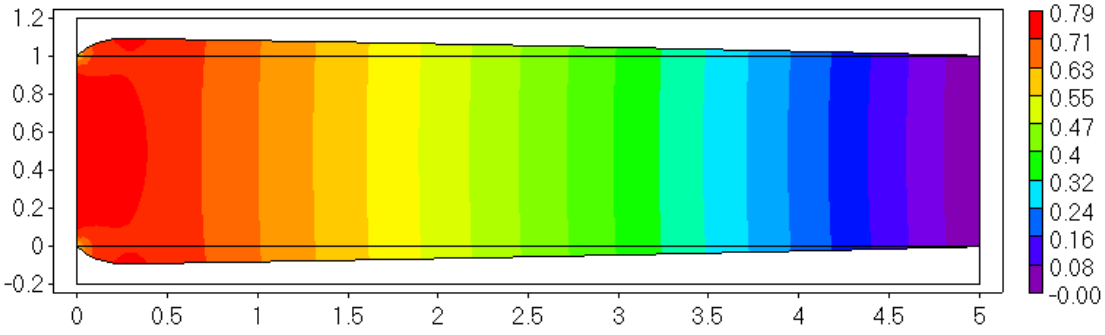

(a) Pressure profile

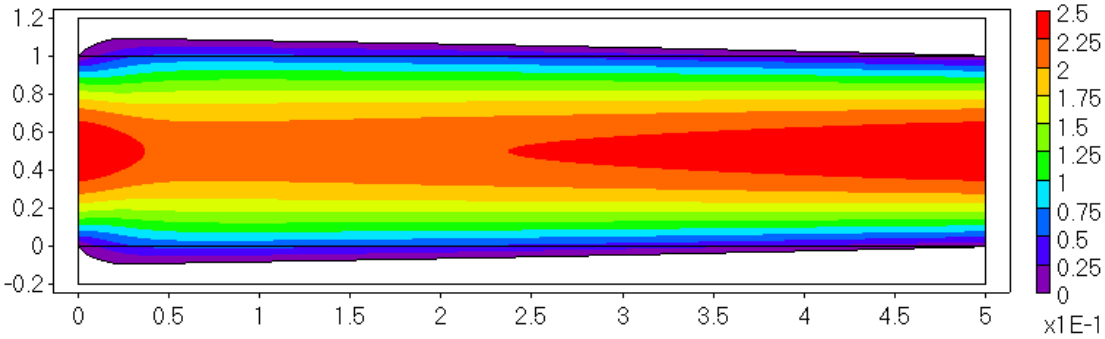

(b) Horizontal velocity profile

FIGURE 6. Solution of the FSI problem for $V_{max} = 1/4$. Shown are the velocity and pressure in the deformed configuration of the fluid domain Ω^f.

TABLE 1

V_{max}	h		$h/2$		$h/4$	
	Iterations	$\max u_y$	Iterations	$\max u_y$	Iterations	$\max u_y$
1/4	9	0.0894687	9	0.0894628	9	0.0894809
1/8	7	0.0504095	7	0.0505136	7	0.0505101
1/16	6	0.0271444	6	0.0271742	6	0.0271846
1/32	5	0.0141473	5	0.0141589	5	0.0141654
1/64	5	0.0072323	5	0.0072312	5	0.0072402

mesh parameters. Finally, since the maximum displacement of the interface for each case of inlet velocity stabilizes as h decreases on can infer that the algorithm is convergent. The next example verifies this by using the asymptotic solution developed in Section 3.

5.2. **Permeability of a long elastic channel.** While the figures presented in the previous numerical example look reasonable from a physical stand point, in the absence of exact analytical solutions it is difficult to verify the quality of the numerical solution. It may

happen that the continuous problem (75) is not well posed. It may also happen that the selected numerical approximation (80)-(82) is not a stable one, that is, the stationary FSI problem (75) does have a unique solution but the FEM subspaces (80)-(82) do not lead to a convergent method.

The asymptotic solution developed in Section 3 for a long elastic channel can however be compared with a numerical one. The asymptotic formulae (65) and (68) are derived based on several assumptions (see Section 3) and without analysis of the rate of convergence with respect to the small parameter ε. However if both the asymptotic solution and the numerical one converge to the actual one, then we should also observe convergence between the two of them. In this section we use the numerical method described in Section 4.3 in order to validate the asymptotic formulae (65) and (68) and vice-versa.

To do this, the elastic channel of Figure 2 is discretized for $l = \delta = 0.5$. In this way, a y-periodic arrangement of this geometry will have solid and fluid regions of equal unit width. The boundary conditions are also modified, compared to the previous model problem. Instead of fixing both displacements at $x = 0$ and $x = L$ we only constrain u_1, i.e. the end of the channel is now free to move in the vertical direction. Note that this does not represent a y-periodic boundary value problem in, because $u_1 = 0$ at $y = \pm(l + \delta)$. Also, the boundary condition for the fluid at the inlet $x = 0$ is a prescribed pressure, i.e, $p(0, y) = P^0$. As in Section 3 the half-width of the channel in the deformed configuration is denoted by $\gamma(x)$.

The asymptotic expansion depends on two parameters - P^0 and $\varepsilon = l/L$. Several numerical results comparing the computed values for γ_h, K_h with the analytical ones γ, K are given in Tables 2 and 3. The first shows the L^2 norm of the error and the second one - the error at a fixed point $x = 0.2 * L$. The numerical solutions used were consequently refined, until the discretization error did not influence the first two digits of the results. It can be seen

TABLE 2. L^2 error along the interface between the numerical and asymptotic results of a long elastic channel.

P^0	$\varepsilon = 10$ $(l = 0.5, L = 5)$		$\varepsilon = 20$ $(l = 0.5, L = 10)$	
	$\frac{\|\gamma_h - \gamma\|_{L^2}}{\|\gamma\|_{L^2}}$	$\frac{\|K_h - K\|}{K}$	$\frac{\|\gamma_h - \gamma\|_{L^2}}{\|\gamma\|_{L^2}}$	$\frac{\|K_h - K\|}{K}$
0.32	2.41×10^{-3}	6.63×10^{-3}	8.47×10^{-4}	1.82×10^{-3}
0.16	1.19×10^{-3}	3.33×10^{-3}	4.21×10^{-4}	1.06×10^{-3}
0.08	5.96×10^{-4}	1.65×10^{-3}	2.10×10^{-4}	5.34×10^{-4}
0.04	2.98×10^{-4}	8.19×10^{-4}	1.05×10^{-4}	2.68×10^{-4}

from Table 2 that formulae (65) and (68) are in very good agreement with the numerically computed solution to the FSI problem. This indicates that as $\varepsilon \to 0$ and $h \to 0$ both the asymptotic and numerical solution to the FSI problem converge to the actual one.

5.3. **Flow through a channel with elastic segment.** In this problem a channel with a deformable segment (Figure 7) is considered. The channel has height $H = 1$ and length $L = 14$ and an elastic segment is located in the middle of the top channel wall. The segment has of length 10, thickness 0.1 and elastic properties $E = 12 * 10^6$ and $\nu = 0.2$. The fluid viscosity and density are again $\mu = \rho = 1$. The segment is built into the rest of the wall at its two ends. The appropriate boundary conditions at the ends of the segment are therefore homogeneous Dirichlet boundary conditions for both displacements. Natural

TABLE 3. Point-wise comparisons of numerical and asymptotic results of a long elastic channel.

P^0	$\varepsilon = 10$ $(l = 0.5, L = 5)$		$\varepsilon = 20$ $(l = 0.5, L = 10)$	
	$\frac{\lvert\gamma_h(1)-\gamma(1)\rvert}{\lvert\gamma(1)\rvert}$	$\frac{\lvert K_h(1)-K(1)\rvert}{\lvert K(1)\rvert}$	$\frac{\lvert\gamma_h(2)-\gamma(2)\rvert}{\lvert\gamma(2)\rvert}$	$\frac{\lvert K_h(2)-K(2)\rvert}{\lvert K(2)\rvert}$
0.32	2.59×10^{-4}	6.02×10^{-4}	8.97×10^{-5}	2.57×10^{-4}
0.16	4.58×10^{-5}	1.71×10^{-5}	2.49×10^{-5}	8.15×10^{-5}
0.08	5.02×10^{-6}	5.79×10^{-5}	5.85×10^{-6}	6.56×10^{-6}
0.04	1.06×10^{-5}	4.38×10^{-5}	4.76×10^{-7}	1.00×10^{-6}

boundary conditions (zero tractions) are imposed on the top side of the segment. The lower side is the fluid-structure interface Γ_0^I. The input flow velocity is again a developed Poiseuille flow: $v_x = \frac{6}{14}Qy(1-y)$, with

$$Q = \int_\Omega v_x d\mathbf{x}$$

being the total volumetric flow rate. The right end of the channel has an outflow boundary condition ($\mathbf{T}^f = \mathbf{0}$). The purpose of this problem is to investigate the permeability of

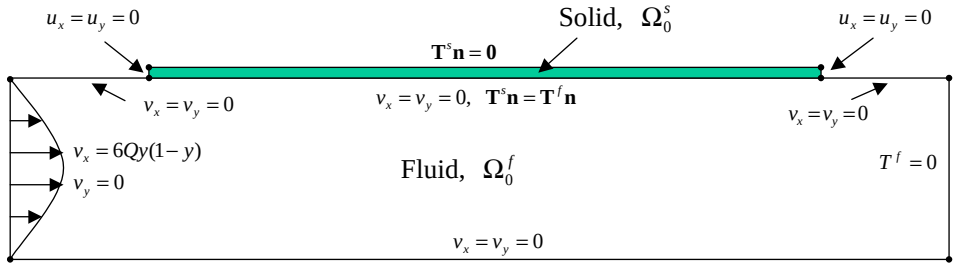

FIGURE 7. Geometry of a channel with an elastic segment (Figure not drawn to scale).

the channel at various values for Q. In the case of an entirely rigid channel the pressure drop $\Delta p/L$ is proportional to the mass flux Q. Since the coupled problem is nonlinear it is expected that for sufficiently large deformations of the interface the resulting mass flow for a given pressure drop will depart from the linear relationship of the Darcy law. The fluid structure problem is solved for several different values of Q and the resulting pressure, pressure gradients in the fluid and displacements in the solid are computed. Two measures for permeability are considered. One is the ratio of the average velocity and average pressure gradient:

$$\bar{K} = \frac{Q}{\int_\Omega \frac{\partial p}{\partial x} d\mathbf{x}}$$

which is similar to the standard homogenization results for flow through rigid skeleton. Since the geometry allows only nonzero net flow in the x direction it also makes sense to consider the pressure drop as an alternative the average pressure gradient:

$$\hat{K} = \frac{Q}{\Delta p/L}.$$

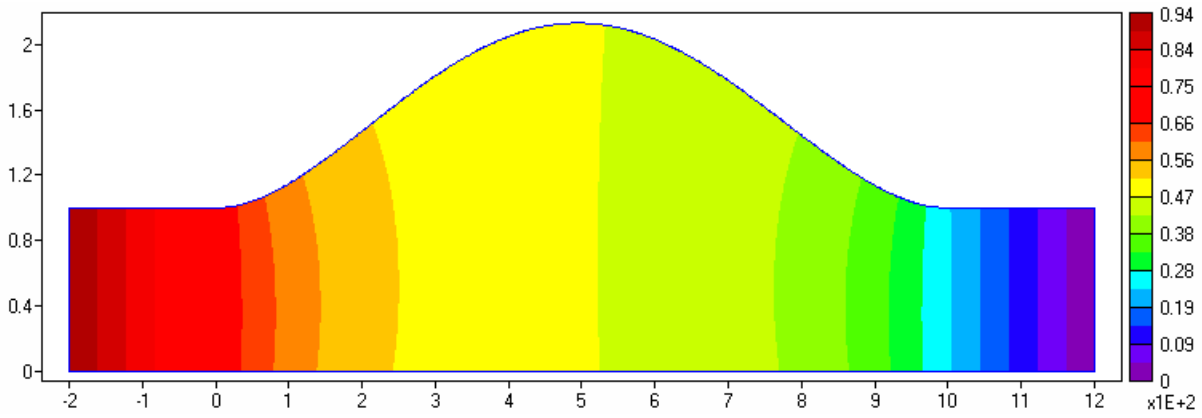

(a) Pressure profile (Figure not drawn to scale).

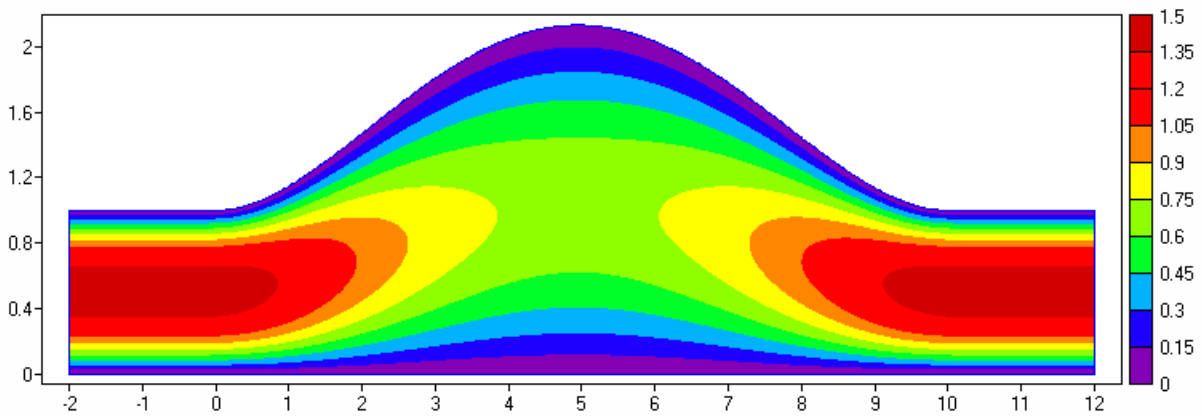

(b) Profile of the horizontal velocity component (Figure not drawn to scale).

FIGURE 8. Final configuration of the fluid domain Ω^f for $Q = 15$.

While the pressure gradient can be readily calculated from the flow solution, it is not immediately clear how to evaluate the pressure drop across the channel. However, thanks to the selection of material parameters and geometry dimensions the inlet is sufficiently away from the segment so the change in the flow downstream does not affect much the inlet pressure distribution, which is essentially constant along the y direction. Similarly, the outlet is sufficiently separated from the end of the elastic segment and the flow has time to redevelop to the parabolic Poiseuille distribution as can be seen on Figures 8(a) and 8(b). The results are summarized on Table 4 and it is clear that both permeability measures behave nonlinearly as Q is varied. This can also be seen on Figure 9 which shows $\bar{K}$ and $\hat{K}$ as functions of Q. As $Q \to 0$ both of them tend to the permeability of a straight, rigid channel which can be calculated directly from the Poiseuille solution and in this case is equal to $1/12$.

TABLE 4

Q	$\int_\Omega \frac{\partial p}{\partial x} d\mathbf{x}$	$p\|_{inlet}$	$Q/\int_\Omega \frac{\partial p}{\partial x} d\mathbf{x}$	$\frac{Q}{\Delta p/L}$	$\max u_y$
14.0000	-106.0853266	-93.8605	0.13196	0.14916	1.161
7.0000	-60.3754287	-53.9478	0.11594	0.12975	0.651
3.5000	-33.6888175	-30.8411	0.10389	0.11348	0.373
1.7500	-18.3178061	-17.2482	0.09553	0.10146	0.209
0.8750	-9.7023494	-9.35044	0.09018	0.09358	0.113
0.4375	-5.0280238	-4.923492	0.08701	0.08889	

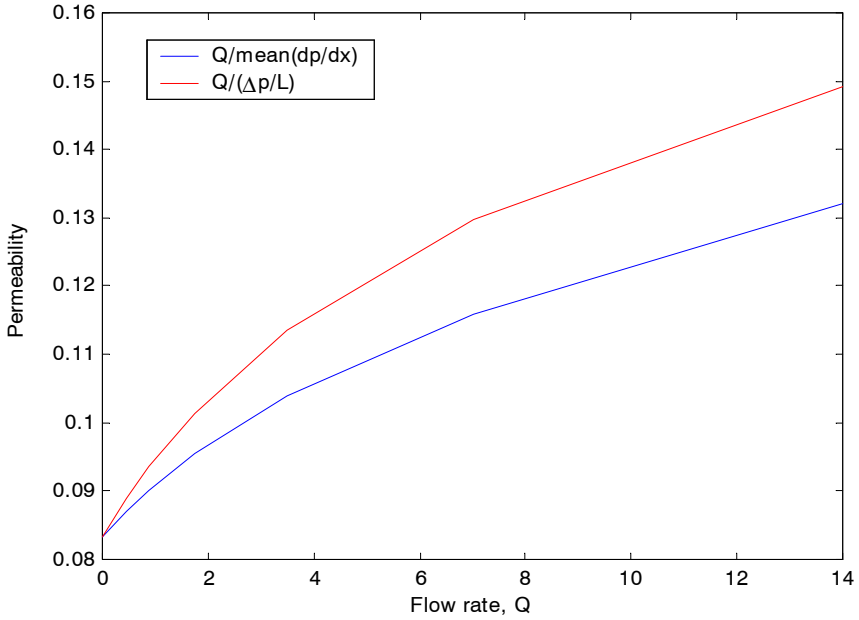

FIGURE 9. Permeability of a channel with elastic segment.

6. CONCLUSIONS

In this paper, a poroelastic medium is considered and the Fluid-Structure Interaction problem at the microscale is presented. The displacements of the fluid-structure interface at the pore level are assumed large enough so that standard homogenization techniques leading to Biot-type equations on the macroscopic scale cannot be applied. An asymptotic analysis is then performed on a long elastic channel and a nonlinear Darcy-type of law for the y-averaged pressure is obtained. From this equation a nonlinear upscaled permeability-like quantity is identified. This permeability is found to depend on the initial channel geometry, Lamé's constants for the solid and the y-averaged pressure in the channel.

An FEM based Fluid-Structure solver is also presented. The solver successfully utilized a Dirichlet-Neumann iterative a scheme for solving the FSI problem. A numerical computation is performed which are used to verify the numerical solutions in comparisons with an asymptotic solution to the FSI problem. This increases the degree of confidence with which

such numerical methods can be used in the absence of solid mathematical understanding of their properties. It also corroborates the asymptotic derivation.

Work on upscaling the poroelasticity problem and the related FSI equations can progress in multiple directions. When no restrictions are placed on the pore-level displacements, it is unlikely that closed-form macroscopic equations can be obtained for general geometries. However, numerical upscaling can be attempted and the analysis in this work suggest that the average pressure at the pore-level should be the most important upscaling parameter. Further, it will be helpful to compare microscale solutions to the FSI problem with macroscopic solutions of various macroscopic poroelastic equation and determine when the standard homogenization fails.

The iterative algorithm for the FSI problem can also be improved. At the end of each solid solve it can be attempted to perform a line-search along the direction of the proposed interface displacement and try to correct it so that certain residual is always reduced. It can also be attempted to keep track of several possible interface correction displacements and favor new interface positions which are orthogonal to past displacements. Such work can improve both the convergence rate and the stability of the algorithm.

Acknowledgments

This work was made possible with the financial support of the Fraunhofer Institut für Techno- und Wirtschaftsmathematik in Kaiserslautern, Germany and the Air Force Office of Scientific Research, USA. Peter Popov would also like to express deep gratitude to Dr. Heiko Andrä for guidance and advice during this project. The work of O.Iliev has been partially supported by EC under the project INTAS-30-50-4395.

References

1. J.-L. Auriault and E. Sanchez-Palencia, *Étude du comportement macroscopique d'un milieu poreux saturé déformable*, Journal de Mécanique **16** (1977), 575–603.
2. O. Axelsson and M. Neytcheva, *Preconditioning methods for linear systems arising in constrained optimiziation problems*, Numerical Linear Algerba with Applications **10** (2003), 3–31.
3. N. Bakhvalov and G. Panasenko, *Homogenization: Averaging processes in periodic media*, Kluwer Academic Publishers, Dordrecht, 1990.
4. J. Bear, *Dynamics of fluids in porous media*, Dover, New York, 1972.
5. A. Bensoussan, J.L. Lions, and G. Papanicolaou, *Assymptotic analysis for periodic structures*, Studies in Mathematics and Its Applications, vol. 5, North-Holland, Amsterdam, 1978.
6. M.A. Biot, *General theory of three dimensional consolidation*, J. Appl. Phys. **12** (1941), 155–164.
7. R. Blaheta, *Displacement decompostion - incomplete factorization preconditioning rechniques for linear elasticity problems*, Numerical Linear Algebra with Applications **1** (1994), 107–128.
8. J. Bramble and J. Pasciak, *Iterative techniques for time dependent stokes problems*, Computers and Mathematics with Applications **33** (1997), no. 1/2, 13–30.
9. V. Girault and P.A. Raviart, *Finite element methods for navier-stokes equations*, Springer-Verlag, Berlin, 1986.
10. G. H. Golub and C. F. Van Loan, *Matrix computations*, Johns Hopkins University Press, Baltimore, 1996.
11. P. M. Gresho and R. L. Sani, *Incompressible flow and the finite element method: Advection - diffusion and isothermal laminar flow*, John Wiley & Sons, Inc, Chichester, UK, 1998.
12. Morton E. Gurtin, *An introduction to continuum mechanics*, Academics Press, San Diego, CA, 1981.
13. M.R. Hesteness and E.L. Stiefel, *Methods of conjugate gradients for solving linear systems*, Journal of Research of the National Bureau of Standards, Section B **49** (1952), 409–436.

14. C. Lanczos, *Solution of systems of linear equations by minimized iterations*, Journal of Research of the National Bureau of Standards **49** (1952), 33–53.
15. Cheo K. Lee and Chiang C. Mei, *Re-examination of the equations of poroelasticity*, Int. J. Eng. Sci. **35** (1997), 329–352.
16. J.L. Lions and Magenes, *Problèmes aux limites non homogènes et applications*, vol. 1, Dunod, Paris, 1968.
17. L. E. Malvern, *Introduction to the mechanics of a continuous medium*, Prentice-Hall, Inc., Englewood Cliffs, NJ, 1969.
18. C.C. Mei and J.-L. Auriault, *Mechanics of heterogeneous porous media with several spatial scales*, Proc. Roy. Soc. Lond. A **426** (1989), 391–423.
19. J. Nečas and I. Hlaváček, *Mathematical theory of elastic and elasto-plastic bodies*, Elsevier, Amsterdam, 1981.
20. Y. Saad, *Iterative methods for sparse linear systems*, PWS, New York, 1996.
21. E. Sanchez-Palencia, *Non-homogeneous media and vibration theory*, Lecture Notes in Physics, vol. 127, Springer-Verlag, Berlin, 1980.
22. S. Turek, *Efficient solvers for incompressible flow problems: An algorithmic and computational approach*, Springer Verlag, New York, 1999.
23. V.V Zhikov, S.M. Kozlov, and O.A. Oleinik, *Homogenization of differential operators and integral functionals*, Springer-Verlag, Berlin, 1994.

Fraunhofer Institut für Techno- und Wirtschaftsmathematik, D-67657 Kaiserslautern, Germany
E-mail address: iliev@itwm.fhg.de

UFR Mathmatiques LaPCS, Bt. Doyen Jean Braconnier,, Universit Claude Bernard Lyon 1, 21, avenue Claude Bernard, 69622 Villeurbanne Cedex
E-mail address: amikelic@free.fr

Department of Aerospace Engineering Texas A&M University, College Station, TX 77843, USA
E-mail address: ppopov@tamu.edu

Published reports of the Fraunhofer ITWM

The PDF-files of the following reports are available under:
www.itwm.fraunhofer.de/de/zentral__berichte/berichte

1. D. Hietel, K. Steiner, J. Struckmeier

A Finite - Volume Particle Method for Compressible Flows

We derive a new class of particle methods for conservation laws, which are based on numerical flux functions to model the interactions between moving particles. The derivation is similar to that of classical Finite-Volume methods; except that the fixed grid structure in the Finite-Volume method is substituted by so-called mass packets of particles. We give some numerical results on a shock wave solution for Burgers equation as well as the well-known one-dimensional shock tube problem.
(19 pages, 1998)

2. M. Feldmann, S. Seibold

Damage Diagnosis of Rotors: Application of Hilbert Transform and Multi-Hypothesis Testing

In this paper, a combined approach to damage diagnosis of rotors is proposed. The intention is to employ signal-based as well as model-based procedures for an improved detection of size and location of the damage. In a first step, Hilbert transform signal processing techniques allow for a computation of the signal envelope and the instantaneous frequency, so that various types of non-linearities due to a damage may be identified and classified based on measured response data. In a second step, a multi-hypothesis bank of Kalman Filters is employed for the detection of the size and location of the damage based on the information of the type of damage provided by the results of the Hilbert transform.
Keywords: Hilbert transform, damage diagnosis, Kalman filtering, non-linear dynamics
(23 pages, 1998)

3. Y. Ben-Haim, S. Seibold

Robust Reliability of Diagnostic Multi-Hypothesis Algorithms: Application to Rotating Machinery

Damage diagnosis based on a bank of Kalman filters, each one conditioned on a specific hypothesized system condition, is a well recognized and powerful diagnostic tool. This multi-hypothesis approach can be applied to a wide range of damage conditions. In this paper, we will focus on the diagnosis of cracks in rotating machinery. The question we address is: how to optimize the multi-hypothesis algorithm with respect to the uncertainty of the spatial form and location of cracks and their resulting dynamic effects. First, we formulate a measure of the reliability of the diagnostic algorithm, and then we discuss modifications of the diagnostic algorithm for the maximization of the reliability. The reliability of a diagnostic algorithm is measured by the amount of uncertainty consistent with no-failure of the diagnosis. Uncertainty is quantitatively represented with convex models.
Keywords: Robust reliability, convex models, Kalman filtering, multi-hypothesis diagnosis, rotating machinery, crack diagnosis
(24 pages, 1998)

4. F.-Th. Lentes, N. Siedow

Three-dimensional Radiative Heat Transfer in Glass Cooling Processes

For the numerical simulation of 3D radiative heat transfer in glasses and glass melts, practically applicable mathematical methods are needed to handle such problems optimal using workstation class computers. Since the exact solution would require super-computer capabilities we concentrate on approximate solutions with a high degree of accuracy. The following approaches are studied: 3D diffusion approximations and 3D ray-tracing methods.
(23 pages, 1998)

5. A. Klar, R. Wegener

A hierarchy of models for multilane vehicular traffic
Part I: Modeling

In the present paper multilane models for vehicular traffic are considered. A microscopic multilane model based on reaction thresholds is developed. Based on this model an Enskog like kinetic model is developed. In particular, care is taken to incorporate the correlations between the vehicles. From the kinetic model a fluid dynamic model is derived. The macroscopic coefficients are deduced from the underlying kinetic model. Numerical simulations are presented for all three levels of description in [10]. Moreover, a comparison of the results is given there.
(23 pages, 1998)

Part II: Numerical and stochastic investigations

In this paper the work presented in [6] is continued. The present paper contains detailed numerical investigations of the models developed there. A numerical method to treat the kinetic equations obtained in [6] are presented and results of the simulations are shown. Moreover, the stochastic correlation model used in [6] is described and investigated in more detail.
(17 pages, 1998)

6. A. Klar, N. Siedow

Boundary Layers and Domain Decomposition for Radiative Heat Transfer and Diffusion Equations: Applications to Glass Manufacturing Processes

In this paper domain decomposition methods for radiative transfer problems including conductive heat transfer are treated. The paper focuses on semi-transparent materials, like glass, and the associated conditions at the interface between the materials. Using asymptotic analysis we derive conditions for the coupling of the radiative transfer equations and a diffusion approximation. Several test cases are treated and a problem appearing in glass manufacturing processes is computed. The results clearly show the advantages of a domain decomposition approach. Accuracy equivalent to the solution of the global radiative transfer solution is achieved, whereas computation time is strongly reduced.
(24 pages, 1998)

7. I. Choquet

Heterogeneous catalysis modelling and numerical simulation in rarified gas flows
Part I: Coverage locally at equilibrium

A new approach is proposed to model and simulate numerically heterogeneous catalysis in rarefied gas flows. It is developed to satisfy all together the following points:
1) describe the gas phase at the microscopic scale, as required in rarefied flows,
2) describe the wall at the macroscopic scale, to avoid prohibitive computational costs and consider not only crystalline but also amorphous surfaces,
3) reproduce on average macroscopic laws correlated with experimental results and
4) derive analytic models in a systematic and exact way. The problem is stated in the general framework of a non static flow in the vicinity of a catalytic and non porous surface (without aging). It is shown that the exact and systematic resolution method based on the Laplace transform, introduced previously by the author to model collisions in the gas phase, can be extended to the present problem. The proposed approach is applied to the modelling of the EleyRideal and LangmuirHinshelwood recombinations, assuming that the coverage is locally at equilibrium. The models are developed considering one atomic species and extended to the general case of several atomic species. Numerical calculations show that the models derived in this way reproduce with accuracy behaviors observed experimentally.
(24 pages, 1998)

8. J. Ohser, B. Steinbach, C. Lang

Efficient Texture Analysis of Binary Images

A new method of determining some characteristics of binary images is proposed based on a special linear filtering. This technique enables the estimation of the area fraction, the specific line length, and the specific integral of curvature. Furthermore, the specific length of the total projection is obtained, which gives detailed information about the texture of the image. The influence of lateral and directional resolution depending on the size of the applied filter mask is discussed in detail. The technique includes a method of increasing directional resolution for texture analysis while keeping lateral resolution as high as possible.
(17 pages, 1998)

9. J. Orlik

Homogenization for viscoelasticity of the integral type with aging and shrinkage

A multiphase composite with periodic distributed inclusions with a smooth boundary is considered in this contribution. The composite component materials are supposed to be linear viscoelastic and aging (of the nonconvolution integral type, for which the Laplace transform with respect to time is not effectively applicable) and are subjected to isotropic shrinkage. The free shrinkage deformation can be considered as a fictitious temperature deformation in the behavior law. The procedure presented in this paper proposes a way to determine average (effective homogenized) viscoelastic and shrinkage (temperature) composite properties and the homogenized stressfield from known properties of the components. This is done by the extension of the asymptotic homogenization technique known for pure elastic nonhomogeneous bodies to the nonhomogeneous thermoviscoelasticity of the integral nonconvolution type. Up to now, the homogenization theory has not covered viscoelasticity of the integral type. SanchezPalencia (1980), Francfort & Suquet (1987) (see [2], [9]) have considered homogenization for viscoelasticity of the differential form and only up to the first derivative order. The integralmodeled viscoelasticity is more general then the differential one and includes almost all known differential models. The homogenization procedure is based on the construction of an asymptotic solution with respect to a period of the composite structure. This reduces the original problem to some auxiliary boundary value problems of elasticity and viscoelasticity on the unit periodic cell, of the same type as the original non-homogeneous problem. The existence and uniqueness results for such problems were obtained for kernels satisfying some constrain conditions. This is done by the extension of the Volterra integral operator theory to the Volterra operators with respect to the time, whose 1 kernels are space linear operators for any fixed time variables. Some ideas of such approach were proposed in [11] and [12], where the Volterra operators with kernels depending additionally on parameter were considered. This manuscript delivers results of the same nature for the case of the spaceoperator kernels.
(20 pages, 1998)

10. J. Mohring

Helmholtz Resonators with Large Aperture

The lowest resonant frequency of a cavity resonator is usually approximated by the classical Helmholtz formula. However, if the opening is rather large and the front wall is narrow this formula is no longer valid. Here we present a correction which is of third order in the ratio of the diameters of aperture and cavity. In addition to the high accuracy it allows to estimate the damping due to radiation. The result is found by applying the method of matched asymptotic expansions. The correction contains form factors describing the shapes of opening and cavity. They are computed for a number of standard geometries. Results are compared with

numerical computations.
(21 pages, 1998)

11. H. W. Hamacher, A. Schöbel

On Center Cycles in Grid Graphs

Finding "good" cycles in graphs is a problem of great interest in graph theory as well as in locational analysis. We show that the center and median problems are NP hard in general graphs. This result holds both for the variable cardinality case (i.e. all cycles of the graph are considered) and the fixed cardinality case (i.e. only cycles with a given cardinality p are feasible). Hence it is of interest to investigate special cases where the problem is solvable in polynomial time. In grid graphs, the variable cardinality case is, for instance, trivially solvable if the shape of the cycle can be chosen freely. If the shape is fixed to be a rectangle one can analyze rectangles in grid graphs with, in sequence, fixed dimension, fixed cardinality, and variable cardinality. In all cases a complete characterization of the optimal cycles and closed form expressions of the optimal objective values are given, yielding polynomial time algorithms for all cases of center rectangle problems. Finally, it is shown that center cycles can be chosen as rectangles for small cardinalities such that the center cycle problem in grid graphs is in these cases completely solved.
(15 pages, 1998)

12. H. W. Hamacher, K.-H. Küfer

Inverse radiation therapy planning - a multiple objective optimisation approach

For some decades radiation therapy has been proved successful in cancer treatment. It is the major task of clinical radiation treatment planning to realize on the one hand a high level dose of radiation in the cancer tissue in order to obtain maximum tumor control. On the other hand it is obvious that it is absolutely necessary to keep in the tissue outside the tumor, particularly in organs at risk, the unavoidable radiation as low as possible.
No doubt, these two objectives of treatment planning - high level dose in the tumor, low radiation outside the tumor - have a basically contradictory nature. Therefore, it is no surprise that inverse mathematical models with dose distribution bounds tend to be infeasible in most cases. Thus, there is need for approximations compromising between overdosing the organs at risk and underdosing the target volume.
Differing from the currently used time consuming iterative approach, which measures deviation from an ideal (non-achievable) treatment plan using recursively trial-and-error weights for the organs of interest, we go a new way trying to avoid a priori weight choices and consider the treatment planning problem as a multiple objective linear programming problem: with each organ of interest, target tissue as well as organs at risk, we associate an objective function measuring the maximal deviation from the prescribed doses.
We build up a data base of relatively few efficient solutions representing and approximating the variety of Pareto solutions of the multiple objective linear programming problem. This data base can be easily scanned by physicians looking for an adequate treatment plan with the aid of an appropriate online tool.
(14 pages, 1999)

13. C. Lang, J. Ohser, R. Hilfer

On the Analysis of Spatial Binary Images

This paper deals with the characterization of microscopically heterogeneous, but macroscopically homogeneous spatial structures. A new method is presented which is strictly based on integral-geometric formulae such as Crofton's intersection formulae and Hadwiger's recursive definition of the Euler number. The corresponding algorithms have clear advantages over other techniques. As an example of application we consider the analysis of spatial digital images produced by means of Computer Assisted Tomography.
(20 pages, 1999)

14. M. Junk

On the Construction of Discrete Equilibrium Distributions for Kinetic Schemes

A general approach to the construction of discrete equilibrium distributions is presented. Such distribution functions can be used to set up Kinetic Schemes as well as Lattice Boltzmann methods. The general principles are also applied to the construction of Chapman Enskog distributions which are used in Kinetic Schemes for compressible Navier-Stokes equations.
(24 pages, 1999)

15. M. Junk, S. V. Raghurame Rao

A new discrete velocity method for Navier-Stokes equations

The relation between the Lattice Boltzmann Method, which has recently become popular, and the Kinetic Schemes, which are routinely used in Computational Fluid Dynamics, is explored. A new discrete velocity model for the numerical solution of Navier-Stokes equations for incompressible fluid flow is presented by combining both the approaches. The new scheme can be interpreted as a pseudo-compressibility method and, for a particular choice of parameters, this interpretation carries over to the Lattice Boltzmann Method.
(20 pages, 1999)

16. H. Neunzert

Mathematics as a Key to Key Technologies

The main part of this paper will consist of examples, how mathematics really helps to solve industrial problems; these examples are taken from our Institute for Industrial Mathematics, from research in the Technomathematics group at my university, but also from ECMI groups and a company called TecMath, which originated 10 years ago from my university group and has already a very successful history.
(39 pages (4 PDF-Files), 1999)

17. J. Ohser, K. Sandau

Considerations about the Estimation of the Size Distribution in Wicksell's Corpuscle Problem

Wicksell's corpuscle problem deals with the estimation of the size distribution of a population of particles, all having the same shape, using a lower dimensional sampling probe. This problem was originary formulated for particle systems occurring in life sciences but its solution is of actual and increasing interest in materials science. From a mathematical point of view, Wicksell's problem is an inverse problem where the interesting size distribution is the unknown part of a Volterra equation. The problem is often regarded ill-posed, because the structure of the integrand implies unstable numerical solutions. The accuracy of the numerical solutions is considered here using the condition number, which allows to compare different numerical methods with different (equidistant) class sizes and which indicates, as one result, that a finite section thickness of the probe reduces the numerical problems. Furthermore, the relative error of estimation is computed which can be split into two parts. One part consists of the relative discretization error that increases for increasing class size, and the second part is related to the relative statistical error which increases with decreasing class size. For both parts, upper bounds can be given and the sum of them indicates an optimal class width depending on some specific constants.
(18 pages, 1999)

18. E. Carrizosa, H. W. Hamacher, R. Klein, S. Nickel

Solving nonconvex planar location problems by finite dominating sets

It is well-known that some of the classical location problems with polyhedral gauges can be solved in polynomial time by finding a finite dominating set, i. e. a finite set of candidates guaranteed to contain at least one optimal location.
In this paper it is first established that this result holds for a much larger class of problems than currently considered in the literature. The model for which this result can be proven includes, for instance, location problems with attraction and repulsion, and location-allocation problems.
Next, it is shown that the approximation of general gauges by polyhedral ones in the objective function of our general model can be analyzed with regard to the subsequent error in the optimal objective value. For the approximation problem two different approaches are described, the sandwich procedure and the greedy algorithm. Both of these approaches lead - for fixed epsilon - to polynomial approximation algorithms with accuracy epsilon for solving the general model considered in this paper.
Keywords: Continuous Location, Polyhedral Gauges, Finite Dominating Sets, Approximation, Sandwich Algorithm, Greedy Algorithm
(19 pages, 2000)

19. A. Becker

A Review on Image Distortion Measures

Within this paper we review image distortion measures. A distortion measure is a criterion that assigns a "quality number" to an image. We distinguish between mathematical distortion measures and those distortion measures in-cooperating a priori knowledge about the imaging devices (e. g. satellite images), image processing algorithms or the human physiology. We will consider representative examples of different kinds of distortion measures and are going to discuss them.
Keywords: Distortion measure, human visual system
(26 pages, 2000)

20. H. W. Hamacher, M. Labbé, S. Nickel, T. Sonneborn

Polyhedral Properties of the Uncapacitated Multiple Allocation Hub Location Problem

We examine the feasibility polyhedron of the uncapacitated hub location problem (UHL) with multiple allocation, which has applications in the fields of air passenger and cargo transportation, telecommunication and postal delivery services. In particular we determine the dimension and derive some classes of facets of this polyhedron. We develop some general rules about lifting facets from the uncapacitated facility location (UFL) for UHL and projecting facets from UHL to UFL. By applying these rules we get a new class of facets for UHL which dominates the inequalities in the original formulation. Thus we get a new formulation of UHL whose constraints are all facet–defining. We show its superior computational performance by benchmarking it on a well known data set.
Keywords: integer programming, hub location, facility location, valid inequalities, facets, branch and cut
(21 pages, 2000)

21. H. W. Hamacher, A. Schöbel

Design of Zone Tariff Systems in Public Transportation

Given a public transportation system represented by its stops and direct connections between stops, we consider two problems dealing with the prices for the customers: The fare problem in which subsets of stops are already aggregated to zones and "good" tariffs have to be found in the existing zone system. Closed form solutions for the fare problem are presented for three objective functions. In the zone problem the design of the zones is part of the problem. This problem is NP hard and we therefore propose three heuristics which prove to be very successful in the redesign of one of Germany's transportation systems.
(30 pages, 2001)

22. D. Hietel, M. Junk, R. Keck, D. Teleaga:

The Finite-Volume-Particle Method for Conservation Laws

In the Finite-Volume-Particle Method (FVPM), the weak formulation of a hyperbolic conservation law is discretized by restricting it to a discrete set of test functions. In contrast to the usual Finite-Volume approach, the test functions are not taken as characteristic functions of the control volumes in a spatial grid, but are chosen from a partition of unity with smooth and overlapping partition functions (the particles), which can even move along pre- scribed velocity fields. The information exchange between particles is based on standard numerical flux functions. Geometrical information, similar to the surface area of the cell faces in the Finite-Volume Method

and the corresponding normal directions are given as integral quantities of the partition functions. After a brief derivation of the Finite-Volume-Particle Method, this work focuses on the role of the geometric coefficients in the scheme.
(16 pages, 2001)

23. T. Bender, H. Hennes, J. Kalcsics, M. T. Melo, S. Nickel

Location Software and Interface with GIS and Supply Chain Management

The objective of this paper is to bridge the gap between location theory and practice. To meet this objective focus is given to the development of software capable of addressing the different needs of a wide group of users. There is a very active community on location theory encompassing many research fields such as operations research, computer science, mathematics, engineering, geography, economics and marketing. As a result, people working on facility location problems have a very diverse background and also different needs regarding the software to solve these problems. For those interested in non-commercial applications (e. g. students and researchers), the library of location algorithms (LoLA can be of considerable assistance. LoLA contains a collection of efficient algorithms for solving planar, network and discrete facility location problems. In this paper, a detailed description of the functionality of LoLA is presented. In the fields of geography and marketing, for instance, solving facility location problems requires using large amounts of demographic data. Hence, members of these groups (e. g. urban planners and sales managers) often work with geographical information too s. To address the specific needs of these users, LoLA was inked to a geographical information system (GIS) and the details of the combined functionality are described in the paper. Finally, there is a wide group of practitioners who need to solve large problems and require special purpose software with a good data interface. Many of such users can be found, for example, in the area of supply chain management (SCM). Logistics activities involved in strategic SCM include, among others, facility location planning. In this paper, the development of a commercial location software tool is also described. The too is embedded in the Advanced Planner and Optimizer SCM software developed by SAP AG, Walldorf, Germany. The paper ends with some conclusions and an outlook to future activities.
Keywords: facility location, software development, geographical information systems, supply chain management.
(48 pages, 2001)

24. H. W. Hamacher, S. A. Tjandra

Mathematical Modelling of Evacuation Problems: A State of Art

This paper details models and algorithms which can be applied to evacuation problems. While it concentrates on building evacuation many of the results are applicable also to regional evacuation. All models consider the time as main parameter, where the travel time between components of the building is part of the input and the overall evacuation time is the output. The paper distinguishes between macroscopic and microscopic evacuation models both of which are able to capture the evacuees' movement over time.
Macroscopic models are mainly used to produce good lower bounds for the evacuation time and do not consider any individual behavior during the emergency situation. These bounds can be used to analyze existing buildings or help in the design phase of planning a building. Macroscopic approaches which are based on dynamic network flow models (minimum cost dynamic flow, maximum dynamic flow, universal maximum flow, quickest path and quickest flow) are described. A special feature of the presented approach is the fact, that travel times of evacuees are not restricted to be constant, but may be density dependent. Using multicriteria optimization priority regions and blockage due to fire or smoke may be considered. It is shown how the modelling can be done using time parameter either as discrete or continuous parameter.
Microscopic models are able to model the individual evacuee's characteristics and the interaction among evacuees which influence their movement. Due to the corresponding huge amount of data one uses simulation approaches. Some probabilistic laws for individual evacuee's movement are presented. Moreover ideas to model the evacuee's movement using cellular automata (CA) and resulting software are presented. In this paper we will focus on macroscopic models and only summarize some of the results of the microscopic approach. While most of the results are applicable to general evacuation situations, we concentrate on building evacuation.
(44 pages, 2001)

25. J. Kuhnert, S. Tiwari

Grid free method for solving the Poisson equation

A Grid free method for solving the Poisson equation is presented. This is an iterative method. The method is based on the weighted least squares approximation in which the Poisson equation is enforced to be satisfied in every iterations. The boundary conditions can also be enforced in the iteration process. This is a local approximation procedure. The Dirichlet, Neumann and mixed boundary value problems on a unit square are presented and the analytical solutions are compared with the exact solutions. Both solutions matched perfectly.
Keywords: Poisson equation, Least squares method, Grid free method
(19 pages, 2001)

26. T. Götz, H. Rave, D. Reinel-Bitzer, K. Steiner, H. Tiemeier

Simulation of the fiber spinning process

To simulate the influence of process parameters to the melt spinning process a fiber model is used and coupled with CFD calculations of the quench air flow. In the fiber model energy, momentum and mass balance are solved for the polymer mass flow. To calculate the quench air the Lattice Boltzmann method is used. Simulations and experiments for different process parameters and hole configurations are compared and show a good agreement.
Keywords: Melt spinning, fiber model, Lattice Boltzmann, CFD
(19 pages, 2001)

27. A. Zemitis

On interaction of a liquid film with an obstacle

In this paper mathematical models for liquid films generated by impinging jets are discussed. Attention is stressed to the interaction of the liquid film with some obstacle. S. G. Taylor [Proc. R. Soc. London Ser. A 253, 313 (1959)] found that the liquid film generated by impinging jets is very sensitive to properties of the wire which was used as an obstacle. The aim of this presentation is to propose a modification of the Taylor's model, which allows to simulate the film shape in cases, when the angle between jets is different from 180°. Numerical results obtained by discussed models give two different shapes of the liquid film similar as in Taylors experiments. These two shapes depend on the regime: either droplets are produced close to the obstacle or not. The difference between two regimes becomes larger if the angle between jets decreases. Existence of such two regimes can be very essential for some applications of impinging jets, if the generated liquid film can have a contact with obstacles.
Keywords: impinging jets, liquid film, models, numerical solution, shape
(22 pages, 2001)

28. I. Ginzburg, K. Steiner

Free surface lattice-Boltzmann method to model the filling of expanding cavities by Bingham Fluids

The filling process of viscoplastic metal alloys and plastics in expanding cavities is modelled using the lattice Boltzmann method in two and three dimensions. These models combine the regularized Bingham model for viscoplastic with a free-interface algorithm. The latter is based on a modified immiscible lattice Boltzmann model in which one species is the fluid and the other one is considered as vacuum. The boundary conditions at the curved liquid-vacuum interface are met without any geometrical front reconstruction from a first-order Chapman-Enskog expansion. The numerical results obtained with these models are found in good agreement with available theoretical and numerical analysis.
Keywords: Generalized LBE, free-surface phenomena, interface boundary conditions, filling processes, Bingham viscoplastic model, regularized models
(22 pages, 2001)

29. H. Neunzert

»Denn nichts ist für den Menschen als Menschen etwas wert, was er nicht mit Leidenschaft tun kann«

Vortrag anlässlich der Verleihung des Akademiepreises des Landes Rheinland-Pfalz am 21.11.2001

Was macht einen guten Hochschullehrer aus? Auf diese Frage gibt es sicher viele verschiedene, fachbezogene Antworten, aber auch ein paar allgemeine Gesichtspunkte: es bedarf der »Leidenschaft« für die Forschung (Max Weber), aus der dann auch die Begeisterung für die Lehre erwächst. Forschung und Lehre gehören zusammen, um die Wissenschaft als lebendiges Tun vermitteln zu können. Der Vortrag gibt Beispiele dafür, wie in angewandter Mathematik Forschungsaufgaben aus praktischen Alltagsproblemstellungen erwachsen, die in die Lehre auf verschiedenen Stufen (Gymnasium bis Graduiertenkolleg) einfließen; er leitet damit auch zu einem aktuellen Forschungsgebiet, der Mehrskalenanalyse mit ihren vielfältigen Anwendungen in Bildverarbeitung, Materialentwicklung und Strömungsmechanik über, was aber nur kurz gestreift wird. Mathematik erscheint hier als eine moderne Schlüsseltechnologie, die aber auch enge Beziehungen zu den Geistes- und Sozialwissenschaften hat.
Keywords: Lehre, Forschung, angewandte Mathematik, Mehrskalenanalyse, Strömungsmechanik
(18 pages, 2001)

30. J. Kuhnert, S. Tiwari

Finite pointset method based on the projection method for simulations of the incompressible Navier-Stokes equations

A Lagrangian particle scheme is applied to the projection method for the incompressible Navier-Stokes equations. The approximation of spatial derivatives is obtained by the weighted least squares method. The pressure Poisson equation is solved by a local iterative procedure with the help of the least squares method. Numerical tests are performed for two dimensional cases. The Couette flow, Poiseuelle flow, decaying shear flow and the driven cavity flow are presented. The numerical solutions are obtained for stationary as well as instationary cases and are compared with the analytical solutions for channel flows. Finally, the driven cavity in a unit square is considered and the stationary solution obtained from this scheme is compared with that from the finite element method.
Keywords: Incompressible Navier-Stokes equations, Meshfree method, Projection method, Particle scheme, Least squares approximation
AMS subject classification: 76D05, 76M28
(25 pages, 2001)

31. R. Korn, M. Krekel

Optimal Portfolios with Fixed Consumption or Income Streams

We consider some portfolio optimisation problems where either the investor has a desire for an a priori specified consumption stream or/and follows a deterministic pay in scheme while also trying to maximize expected utility from final wealth. We derive explicit closed form solutions for continuous and discrete monetary streams. The mathematical method used is classical stochastic control theory.
Keywords: Portfolio optimisation, stochastic control, HJB equation, discretisation of control problems.
(23 pages, 2002)

32. M. Krekel

Optimal portfolios with a loan dependent credit spread

If an investor borrows money he generally has to pay higher interest rates than he would have received, if he had put his funds on a savings account. The classical model of continuous time portfolio optimisation ignores this effect. Since there is obviously a connection between the default probability and the total percentage of wealth, which the investor is in debt, we study portfolio optimisation with a control dependent interest rate. Assuming a logarithmic and a power utility function, respectively, we prove explicit formulae of the optimal control.
Keywords: Portfolio optimisation, stochastic control, HJB equation, credit spread, log utility, power utility, non-linear wealth dynamics
(25 pages, 2002)

33. J. Ohser, W. Nagel, K. Schladitz

The Euler number of discretized sets - on the choice of adjacency in homogeneous lattices

Two approaches for determining the Euler-Poincaré characteristic of a set observed on lattice points are considered in the context of image analysis { the integral geometric and the polyhedral approach. Information about the set is assumed to be available on lattice points only. In order to retain properties of the Euler number and to provide a good approximation of the true Euler number of the original set in the Euclidean space, the appropriate choice of adjacency in the lattice for the set and its background is crucial. Adjacencies are defined using tessellations of the whole space into polyhedrons. In R 3 , two new 14 adjacencies are introduced additionally to the well known 6 and 26 adjacencies. For the Euler number of a set and its complement, a consistency relation holds. Each of the pairs of adjacencies (14:1; 14:1), (14:2; 14:2), (6; 26), and (26; 6) is shown to be a pair of complementary adjacencies with respect to this relation. That is, the approximations of the Euler numbers are consistent if the set and its background (complement) are equipped with this pair of adjacencies. Furthermore, sufficient conditions for the correctness of the approximations of the Euler number are given. The analysis of selected microstructures and a simulation study illustrate how the estimated Euler number depends on the chosen adjacency. It also shows that there is not a uniquely best pair of adjacencies with respect to the estimation of the Euler number of a set in Euclidean space.
Keywords: image analysis, Euler number, neighborhod relationships, cuboidal lattice
(32 pages, 2002)

34. I. Ginzburg, K. Steiner

Lattice Boltzmann Model for Free-Surface flow and Its Application to Filling Process in Casting

A generalized lattice Boltzmann model to simulate free-surface is constructed in both two and three dimensions. The proposed model satisfies the interfacial boundary conditions accurately. A distinctive feature of the model is that the collision processes is carried out only on the points occupied partially or fully by the fluid. To maintain a sharp interfacial front, the method includes an anti-diffusion algorithm. The unknown distribution functions at the interfacial region are constructed according to the first order Chapman-Enskog analysis. The interfacial boundary conditions are satisfied exactly by the coefficients in the Chapman-Enskog expansion. The distribution functions are naturally expressed in the local interfacial coordinates. The macroscopic quantities at the interface are extracted from the least-square solutions of a locally linearized system obtained from the known distribution functions. The proposed method does not require any geometric front construction and is robust for any interfacial topology. Simulation results of realistic filling process are presented: rectangular cavity in two dimensions and Hammer box, Campbell box, Sheffield box, and Motorblock in three dimensions. To enhance the stability at high Reynolds numbers, various upwind-type schemes are developed. Free-slip and no-slip boundary conditions are also discussed.
Keywords: Lattice Boltzmann models; free-surface phenomena; interface boundary conditions; filling processes; injection molding; volume of fluid method; interface boundary conditions; advection-schemes; upwind-schemes
(54 pages, 2002)

35. M. Günther, A. Klar, T. Materne, R. Wegener

Multivalued fundamental diagrams and stop and go waves for continuum traffic equations

In the present paper a kinetic model for vehicular traffic leading to multivalued fundamental diagrams is developed and investigated in detail. For this model phase transitions can appear depending on the local density and velocity of the flow. A derivation of associated macroscopic traffic equations from the kinetic equation is given. Moreover, numerical experiments show the appearance of stop and go waves for highway traffic with a bottleneck.
Keywords: traffic flow, macroscopic equations, kinetic derivation, multivalued fundamental diagram, stop and go waves, phase transitions
(25 pages, 2002)

36. S. Feldmann, P. Lang, D. Prätzel-Wolters

Parameter influence on the zeros of network determinants

To a network N(q) with determinant D(s;q) depending on a parameter vector $q \in R^r$ via identification of some of its vertices, a network N^ (q) is assigned. The paper deals with procedures to find N^ (q), such that its determinant D^ (s;q) admits a factorization in the determinants of appropriate subnetworks, and with the estimation of the deviation of the zeros of D^ from the zeros of D. To solve the estimation problem state space methods are applied.
Keywords: Networks, Equicofactor matrix polynomials, Realization theory, Matrix perturbation theory
(30 pages, 2002)

37. K. Koch, J. Ohser, K. Schladitz

Spectral theory for random closed sets and estimating the covariance via frequency space

A spectral theory for stationary random closed sets is developed and provided with a sound mathematical basis. Definition and proof of existence of the Bartlett spectrum of a stationary random closed set as well as the proof of a Wiener-Khintchine theorem for the power spectrum are used to two ends: First, well known second order characteristics like the covariance can be estimated faster than usual via frequency space. Second, the Bartlett spectrum and the power spectrum can be used as second order characteristics in frequency space. Examples show, that in some cases information about the random closed set is easier to obtain from these characteristics in frequency space than from their real world counterparts.
Keywords: Random set, Bartlett spectrum, fast Fourier transform, power spectrum
(28 pages, 2002)

38. D. d'Humières, I. Ginzburg

Multi-reflection boundary conditions for lattice Boltzmann models

We present a unified approach of several boundary conditions for lattice Boltzmann models. Its general framework is a generalization of previously introduced schemes such as the bounce-back rule, linear or quadratic interpolations, etc. The objectives are two fold: first to give theoretical tools to study the existing boundary conditions and their corresponding accuracy; secondly to design formally third- order accurate boundary conditions for general flows. Using these boundary conditions, Couette and Poiseuille flows are exact solution of the lattice Boltzmann models for a Reynolds number $Re = 0$ (Stokes limit).
Numerical comparisons are given for Stokes flows in periodic arrays of spheres and cylinders, linear periodic array of cylinders between moving plates and for Navier-Stokes flows in periodic arrays of cylinders for $Re < 200$. These results show a significant improvement of the overall accuracy when using the linear interpolations instead of the bounce-back reflection (up to an order of magnitude on the hydrodynamics fields). Further improvement is achieved with the new multi-reflection boundary conditions, reaching a level of accuracy close to the quasi-analytical reference solutions, even for rather modest grid resolutions and few points in the narrowest channels. More important, the pressure and velocity fields in the vicinity of the obstacles are much smoother with multi-reflection than with the other boundary conditions.
Finally the good stability of these schemes is highlighted by some simulations of moving obstacles: a cylinder between flat walls and a sphere in a cylinder.
Keywords: lattice Boltzmann equation, boudary condistions, bounce-back rule, Navier-Stokes equation
(72 pages, 2002)

39. R. Korn

Elementare Finanzmathematik

Im Rahmen dieser Arbeit soll eine elementar gehaltene Einführung in die Aufgabenstellungen und Prinzipien der modernen Finanzmathematik gegeben werden. Insbesondere werden die Grundlagen der Modellierung von Aktienkursen, der Bewertung von Optionen und der Portfolio-Optimierung vorgestellt. Natürlich können die verwendeten Methoden und die entwickelte Theorie nicht in voller Allgemeinheit für den Schulunterricht verwendet werden, doch sollen einzelne Prinzipien so heraus gearbeitet werden, dass sie auch an einfachen Beispielen verstanden werden können.
Keywords: Finanzmathematik, Aktien, Optionen, Portfolio-Optimierung, Börse, Lehrerweiterbildung, Mathematikunterricht
(98 pages, 2002)

40. J. Kallrath, M. C. Müller, S. Nickel

Batch Presorting Problems: Models and Complexity Results

In this paper we consider short term storage systems. We analyze presorting strategies to improve the effiency of these storage systems. The presorting task is called Batch PreSorting Problem (BPSP). The BPSP is a variation of an assigment problem, i. e., it has an assigment problem kernel and some additional constraints. We present different types of these presorting problems, introduce mathematical programming formulations and prove the NP-completeness for one type of the BPSP. Experiments are carried out in order to compare the different model formulations and to investigate the behavior of these models.
Keywords: Complexity theory, Integer programming, Assigment, Logistics
(19 pages, 2002)

41. J. Linn

On the frame-invariant description of the phase space of the Folgar-Tucker equation

The Folgar-Tucker equation is used in flow simulations of fiber suspensions to predict fiber orientation depending on the local flow. In this paper, a complete, frame-invariant description of the phase space of this differential equation is presented for the first time.
Key words: fiber orientation, Folgar-Tucker equation, injection molding
(5 pages, 2003)

42. T. Hanne, S. Nickel

A Multi-Objective Evolutionary Algorithm for Scheduling and Inspection Planning in Software Development Projects

In this article, we consider the problem of planning inspections and other tasks within a software development (SD) project with respect to the objectives quality (no. of defects), project duration, and costs. Based on a discrete-event simulation model of SD processes comprising the phases coding, inspection, test, and rework, we present a simplified formulation of the problem as a multiobjective optimization problem. For solving the problem (i. e. finding an approximation of the efficient set) we develop a multiobjective evolutionary algorithm. Details of the algorithm are discussed as well as results of its application to sample problems.
Key words: multiple objective programming, project

management and scheduling, software development, evolutionary algorithms, efficient set
(29 pages, 2003)

43. T. Bortfeld , K.-H. Küfer, M. Monz, A. Scherrer, C. Thieke, H. Trinkaus

Intensity-Modulated Radiotherapy - A Large Scale Multi-Criteria Programming Problem -

Radiation therapy planning is always a tight rope walk between dangerous insufficient dose in the target volume and life threatening overdosing of organs at risk. Finding ideal balances between these inherently contradictory goals challenges dosimetrists and physicians in their daily practice. Today's planning systems are typically based on a single evaluation function that measures the quality of a radiation treatment plan. Unfortunately, such a one dimensional approach cannot satisfactorily map the different backgrounds of physicians and the patient dependent necessities. So, too often a time consuming iteration process between evaluation of dose distribution and redefinition of the evaluation function is needed.
In this paper we propose a generic multi-criteria approach based on Pareto's solution concept. For each entity of interest - target volume or organ at risk a structure dependent evaluation function is defined measuring deviations from ideal doses that are calculated from statistical functions. A reasonable bunch of clinically meaningful Pareto optimal solutions are stored in a data base, which can be interactively searched by physicians. The system guarantees dynamical planning as well as the discussion of tradeoffs between different entities.
Mathematically, we model the upcoming inverse problem as a multi-criteria linear programming problem. Because of the large scale nature of the problem it is not possible to solve the problem in a 3D-setting without adaptive reduction by appropriate approximation schemes.
Our approach is twofold: First, the discretization of the continuous problem is based on an adaptive hierarchical clustering process which is used for a local refinement of constraints during the optimization procedure. Second, the set of Pareto optimal solutions is approximated by an adaptive grid of representatives that are found by a hybrid process of calculating extreme compromises and interpolation methods.
Keywords: multiple criteria optimization, representative systems of Pareto solutions, adaptive triangulation, clustering and disaggregation techniques, visualization of Pareto solutions, medical physics, external beam radiotherapy planning, intensity modulated radiotherapy
(31 pages, 2003)

44. T. Halfmann, T. Wichmann

Overview of Symbolic Methods in Industrial Analog Circuit Design

Industrial analog circuits are usually designed using numerical simulation tools. To obtain a deeper circuit understanding, symbolic analysis techniques can additionally be applied. Approximation methods which reduce the complexity of symbolic expressions are needed in order to handle industrial-sized problems. This paper will give an overview to the field of symbolic analog circuit analysis. Starting with a motivation, the state-of-the-art simplification algorithms for linear as well as for nonlinear circuits are presented. The basic ideas behind the different techniques are described, whereas the technical details can be found in the cited references. Finally, the application of linear and nonlinear symbolic analysis will be shown on two example circuits.
Keywords: CAD, automated analog circuit design, symbolic analysis, computer algebra, behavioral modeling, system simulation, circuit sizing, macro modeling, differential-algebraic equations, index
(17 pages, 2003)

45. S. E. Mikhailov, J. Orlik

Asymptotic Homogenisation in Strength and Fatigue Durability Analysis of Composites

Asymptotic homogenisation technique and two-scale convergence is used for analysis of macro-strength and fatigue durability of composites with a periodic structure under cyclic loading. The linear damage accumulation rule is employed in the phenomenological micro-durability conditions (for each component of the composite) under varying cyclic loading. Both local and non-local strength and durability conditions are analysed. The strong convergence of the strength and fatigue damage measure as the structure period tends to zero is proved and their limiting values are estimated.
Keywords: multiscale structures, asymptotic homogenization, strength, fatigue, singularity, non-local conditions
(14 pages, 2003)

46. P. Domínguez-Marín, P. Hansen, N. Mladenović, S. Nickel

Heuristic Procedures for Solving the Discrete Ordered Median Problem

We present two heuristic methods for solving the Discrete Ordered Median Problem (DOMP), for which no such approaches have been developed so far. The DOMP generalizes classical discrete facility location problems, such as the p-median, p-center and Uncapacitated Facility Location problems. The first procedure proposed in this paper is based on a genetic algorithm developed by Moreno Vega [MV96] for p-median and p-center problems. Additionally, a second heuristic approach based on the Variable Neighborhood Search metaheuristic (VNS) proposed by Hansen & Mladenovic [HM97] for the p-median problem is described. An extensive numerical study is presented to show the efficiency of both heuristics and compare them.
Keywords: genetic algorithms, variable neighborhood search, discrete facility location
(31 pages, 2003)

47. N. Boland, P. Domínguez-Marín, S. Nickel, J. Puerto

Exact Procedures for Solving the Discrete Ordered Median Problem

The Discrete Ordered Median Problem (DOMP) generalizes classical discrete location problems, such as the N-median, N-center and Uncapacitated Facility Location problems. It was introduced by Nickel [16], who formulated it as both a nonlinear and a linear integer program. We propose an alternative integer linear programming formulation for the DOMP, discuss relationships between both integer linear programming formulations, and show how properties of optimal solutions can be used to strengthen these formulations. Moreover, we present a specific branch and bound procedure to solve the DOMP more efficiently. We test the integer linear programming formulations and this branch and bound method computationally on randomly generated test problems.
Keywords: discrete location, Integer programming
(41 pages, 2003)

48. S. Feldmann, P. Lang

Padé-like reduction of stable discrete linear systems preserving their stability

A new stability preserving model reduction algorithm for discrete linear SISO-systems based on their impulse response is proposed. Similar to the Padé approximation, an equation system for the Markov parameters involving the Hankel matrix is considered, that here however is chosen to be of very high dimension. Although this equation system therefore in general cannot be solved exactly, it is proved that the approximate solution, computed via the Moore-Penrose inverse, gives rise to a stability preserving reduction scheme, a property that cannot be guaranteed for the Padé approach. Furthermore, the proposed algorithm is compared to another stability preserving reduction approach, namely the balanced truncation method, showing comparable performance of the reduced systems. The balanced truncation method however starts from a state space description of the systems and in general is expected to be more computational demanding.
Keywords: Discrete linear systems, model reduction, stability, Hankel matrix, Stein equation
(16 pages, 2003)

49. J. Kallrath, S. Nickel

A Polynomial Case of the Batch Presorting Problem

This paper presents new theoretical results for a special case of the batch presorting problem (BPSP). We will show tht this case can be solved in polynomial time. Offline and online algorithms are presented for solving the BPSP. Competetive analysis is used for comparing the algorithms.
Keywords: batch presorting problem, online optimization, competetive analysis, polynomial algorithms, logistics
(17 pages, 2003)

50. T. Hanne, H. L. Trinkaus

knowCube for MCDM – Visual and Interactive Support for Multicriteria Decision Making

In this paper, we present a novel multicriteria decision support system (MCDSS), called knowCube, consisting of components for knowledge organization, generation, and navigation. Knowledge organization rests upon a database for managing qualitative and quantitative criteria, together with add-on information. Knowledge generation serves filling the database via e.g. identification, optimization, classification or simulation. For "finding needles in haycocks", the knowledge navigation component supports graphical database retrieval and interactive, goal-oriented problem solving. Navigation "helpers" are, for instance, cascading criteria aggregations, modifiable metrics, ergonomic interfaces, and customizable visualizations. Examples from real-life projects, e.g. in industrial engineering and in the life sciences, illustrate the application of our MCDSS.
Key words: Multicriteria decision making, knowledge management, decision support systems, visual interfaces, interactive navigation, real-life applications.
(26 pages, 2003)

51. O. Iliev, V. Laptev

On Numerical Simulation of Flow Through Oil Filters

This paper concerns numerical simulation of flow through oil filters. Oil filters consist of filter housing (filter box), and a porous filtering medium, which completely separates the inlet from the outlet. We discuss mathematical models, describing coupled flows in the pure liquid subregions and in the porous filter media, as well as interface conditions between them. Further, we reformulate the problem in fictitious regions method manner, and discuss peculiarities of the numerical algorithm in solving the coupled system. Next, we show numerical results, validating the model and the algorithm. Finally, we present results from simulation of 3-D oil flow through a real car filter.
Keywords: oil filters, coupled flow in plain and porous media, Navier-Stokes, Brinkman, numerical simulation
(8 pages, 2003)

52. W. Dörfler, O. Iliev, D. Stoyanov, D. Vassileva

On a Multigrid Adaptive Refinement Solver for Saturated Non-Newtonian Flow in Porous Media

A multigrid adaptive refinement algorithm for non-Newtonian flow in porous media is presented. The saturated flow of a non-Newtonian fluid is described by the continuity equation and the generalized Darcy law. The resulting second order nonlinear elliptic equation is discretized by a finite volume method on a cell-centered grid. A nonlinear full-multigrid, full-approximation-storage algorithm is implemented. As a smoother, a single grid solver based on Picard linearization and Gauss-Seidel relaxation is used. Further, a local refinement multigrid algorithm on a composite grid is developed. A residual based error indicator is used in the adaptive refinement criterion. A special implementation

approach is used, which allows us to perform unstructured local refinement in conjunction with the finite volume discretization. Several results from numerical experiments are presented in order to examine the performance of the solver.
Keywords: Nonlinear multigrid, adaptive refinement, non-Newtonian flow in porous media
(17 pages, 2003)

53. S. Kruse

On the Pricing of Forward Starting Options under Stochastic Volatility

We consider the problem of pricing European forward starting options in the presence of stochastic volatility. By performing a change of measure using the asset price at the time of strike determination as a numeraire, we derive a closed-form solution based on Heston's model of stochastic volatility.
Keywords: Option pricing, forward starting options, Heston model, stochastic volatility, cliquet options
(11 pages, 2003)

54. O. Iliev, D. Stoyanov

Multigrid – adaptive local refinement solver for incompressible flows

A non-linear multigrid solver for incompressible Navier-Stokes equations, exploiting finite volume discretization of the equations, is extended by adaptive local refinement. The multigrid is the outer iterative cycle, while the SIMPLE algorithm is used as a smoothing procedure. Error indicators are used to define the refinement subdomain. A special implementation approach is used, which allows to perform unstructured local refinement in conjunction with the finite volume discretization. The multigrid - adaptive local refinement algorithm is tested on 2D Poisson equation and further is applied to a lid-driven flows in a cavity (2D and 3D case), comparing the results with bench-mark data. The software design principles of the solver are also discussed.
Keywords: Navier-Stokes equations, incompressible flow, projection-type splitting, SIMPLE, multigrid methods, adaptive local refinement, lid-driven flow in a cavity
(37 pages, 2003)

55. V. Starikovicius

The multiphase flow and heat transfer in porous media

In first part of this work, summaries of traditional Multiphase Flow Model and more recent Multiphase Mixture Model are presented. Attention is being paid to attempts include various heterogeneous aspects into models. In second part, MMM based differential model for two-phase immiscible flow in porous media is considered. A numerical scheme based on the sequential solution procedure and control volume based finite difference schemes for the pressure and saturation-conservation equations is developed. A computer simulator is built, which exploits object-oriented programming techniques. Numerical result for several test problems are reported.
Keywords: Two-phase flow in porous media, various formulations, global pressure, multiphase mixture model, numerical simulation
(30 pages, 2003)

56. P. Lang, A. Sarishvili, A. Wirsen

Blocked neural networks for knowledge extraction in the software development process

One of the main goals of an organization developing software is to increase the quality of the software while at the same time to decrease the costs and the duration of the development process. To achieve this, various decisions e.ecting this goal before and during the development process have to be made by the managers. One appropriate tool for decision support are simulation models of the software life cycle, which also help to understand the dynamics of the software development process. Building up a simulation model requires a mathematical description of the interactions between di.erent objects involved in the development process. Based on experimental data, techniques from the .eld of knowledge discovery can be used to quantify these interactions and to generate new process knowledge based on the analysis of the determined relationships. In this paper blocked neuronal networks and related relevance measures will be presented as an appropriate tool for quanti.cation and validation of qualitatively known dependencies in the software development process.
Keywords: Blocked Neural Networks, Nonlinear Regression, Knowledge Extraction, Code Inspection
(21 pages, 2003)

57. H. Knaf, P. Lang, S. Zeiser

Diagnosis aiding in Regulation Thermography using Fuzzy Logic

The objective of the present article is to give an overview of an application of Fuzzy Logic in Regulation Thermography, a method of medical diagnosis support. An introduction to this method of the complementary medical science based on temperature measurements – so-called thermograms – is provided. The process of modelling the physician's thermogram evaluation rules using the calculus of Fuzzy Logic is explained.
Keywords: fuzzy logic,knowledge representation, expert system
(22 pages, 2003)

58. M.T. Melo, S. Nickel, F. Saldanha da Gama

Largescale models for dynamic multi-commodity capacitated facility location

In this paper we focus on the strategic design of supply chain networks. We propose a mathematical modeling framework that captures many practical aspects of network design problems simultaneously but which have not received adequate attention in the literature. The aspects considered include: dynamic planning horizon, generic supply chain network structure, external supply of materials, inventory opportunities for goods, distribution of commodities, facility configuration, availability of capital for investments, and storage limitations. Moreover, network configuration decisions concerning the gradual relocation of facilities over the planning horizon are considered. To cope with fluctuating demands, capacity expansion and reduction scenarios are also analyzed as well as modular capacity shifts. The relation of the proposed modeling framework with existing models is discussed. For problems of reasonable size we report on our computational experience with standard mathematical programming software. In particular, useful insights on the impact of various factors on network design decisions are provided.
Keywords: supply chain management, strategic planning, dynamic location, modeling
(40 pages, 2003)

59. J. Orlik

Homogenization for contact problems with periodically rough surfaces

We consider the contact of two elastic bodies with rough surfaces at the interface. The size of the micropeaks and valleys is very small compared with the macrosize of the bodies' domains. This makes the direct application of the FEM for the calculation of the contact problem prohibitively costly. A method is developed that allows deriving a macrocontact condition on the interface. The method involves the twoscale asymptotic homogenization procedure that takes into account the microgeometry of the interface layer and the stiffnesses of materials of both domains. The macrocontact condition can then be used in a FEM model for the contact problem on the macrolevel. The averaged contact stiffness obtained allows the replacement of the interface layer in the macromodel by the macrocontact condition.
Keywords: asymptotic homogenization, contact problems
(28 pages, 2004)

60. A. Scherrer, K.-H. Küfer, M. Monz, F. Alonso, T. Bortfeld

IMRT planning on adaptive volume structures – a significant advance of computational complexity

In intensity-modulated radiotherapy (IMRT) planning the oncologist faces the challenging task of finding a treatment plan that he considers to be an ideal compromise of the inherently contradictive goals of delivering a sufficiently high dose to the target while widely sparing critical structures. The search for this a priori unknown compromise typically requires the computation of several plans, i.e. the solution of several optimization problems. This accumulates to a high computational expense due to the large scale of these problems - a consequence of the discrete problem formulation. This paper presents the adaptive clustering method as a new algorithmic concept to overcome these difficulties. The computations are performed on an individually adapted structure of voxel clusters rather than on the original voxels leading to a decisively reduced computational complexity as numerical examples on real clinical data demonstrate. In contrast to many other similar concepts, the typical trade-off between a reduction in computational complexity and a loss in exactness can be avoided: the adaptive clustering method produces the optimum of the original problem. This flexible method can be applied to both single- and multi-criteria optimization methods based on most of the convex evaluation functions used in practice.
Keywords: Intensity-modulated radiation therapy (IMRT), inverse treatment planning, adaptive volume structures, hierarchical clustering, local refinement, adaptive clustering, convex programming, mesh generation, multi-grid methods
(24 pages, 2004)

61. D. Kehrwald

Parallel lattice Boltzmann simulation of complex flows

After a short introduction to the basic ideas of lattice Boltzmann methods and a brief description of a modern parallel computer, it is shown how lattice Boltzmann schemes are successfully applied for simulating fluid flow in microstructures and calculating material properties of porous media. It is explained how lattice Boltzmann schemes compute the gradient of the velocity field without numerical differentiation. This feature is then utilised for the simulation of pseudo-plastic fluids, and numerical results are presented for a simple benchmark problem as well as for the simulation of liquid composite moulding.
Keywords: Lattice Boltzmann methods, parallel computing, microstructure simulation, virtual material design, pseudo-plastic fluids, liquid composite moulding
(12 pages, 2004)

62. O. Iliev, J. Linn, M. Moog, D. Niedziela, V. Starikovicius

On the Performance of Certain Iterative Solvers for Coupled Systems Arising in Discretization of Non-Newtonian Flow Equations

Iterative solution of large scale systems arising after discretization and linearization of the unsteady non-Newtonian Navier–Stokes equations is studied. cross WLF model is used to account for the non-Newtonian behavior of the fluid. Finite volume method is used to discretize the governing system of PDEs. Viscosity is treated explicitely (e.g., it is taken from the previous time step), while other terms are treated implicitly. Different preconditioners (block–diagonal, block–triangular, relaxed incomplete LU factorization, etc.) are used in conjunction with advanced iterative methods, namely, BiCGStab, CGS, GMRES. The action of the preconditioner in fact requires inverting different blocks. For this purpose, in addition to preconditioned BiCGStab, CGS, GMRES, we use also algebraic multigrid method (AMG). The performance of the iterative solvers is studied with respect to the number of unknowns, characteristic velocity in the basic flow, time step, deviation from Newtonian behavior, etc. Results from numerical experiments are presented and discussed.

Keywords: Performance of iterative solvers, Preconditioners, Non-Newtonian flow
(17 pages, 2004)

63. R. Ciegis, O. Iliev, S. Rief, K. Steiner

On Modelling and Simulation of Different Regimes for Liquid Polymer Moulding

In this paper we consider numerical algorithms for solving a system of nonlinear PDEs arising in modeling of liquid polymer injection. We investigate the particular case when a porous preform is located within the mould, so that the liquid polymer flows through a porous medium during the filling stage. The nonlinearity of the governing system of PDEs is due to the non-Newtonian behavior of the polymer, as well as due to the moving free boundary. The latter is related to the penetration front and a Stefan type problem is formulated to account for it. A finite-volume method is used to approximate the given differential problem. Results of numerical experiments are presented.
We also solve an inverse problem and present algorithms for the determination of the absolute preform permeability coefficient in the case when the velocity of the penetration front is known from measurements. In both cases (direct and inverse problems) we emphasize on the specifics related to the non-Newtonian behavior of the polymer. For completeness, we discuss also the Newtonian case. Results of some experimental measurements are presented and discussed.
Keywords: Liquid Polymer Moulding, Modelling, Simulation, Infiltration, Front Propagation, non-Newtonian flow in porous media
(43 pages, 2004)

64. T. Hanne, H. Neu

Simulating Human Resources in Software Development Processes

In this paper, we discuss approaches related to the explicit modeling of human beings in software development processes. While in most older simulation models of software development processes, esp. those of the system dynamics type, humans are only represented as a labor pool, more recent models of the discrete-event simulation type require representations of individual humans. In that case, particularities regarding the person become more relevant. These individual effects are either considered as stochastic variations of productivity, or an explanation is sought based on individual characteristics, such as skills for instance. In this paper, we explore such possibilities by recurring to some basic results in psychology, sociology, and labor science. Various specific models for representing human effects in software process simulation are discussed.
Keywords: Human resource modeling, software process, productivity, human factors, learning curve
(14 pages, 2004)

65. O. Iliev, A. Mikelic, P. Popov

Fluid structure interaction problems in deformable porous media: Toward permeability of deformable porous media

In this work the problem of fluid flow in deformable porous media is studied. First, the stationary fluid-structure interaction (FSI) problem is formulated in terms of incompressible Newtonian fluid and a linearized elastic solid. The flow is assumed to be characterized by very low Reynolds number and is described by the Stokes equations. The strains in the solid are small allowing for the solid to be described by the Lame equations, but no restrictions are applied on the magnitude of the displacements leading to strongly coupled, nonlinear fluid-structure problem. The FSI problem is then solved numerically by an iterative procedure which solves sequentially fluid and solid subproblems. Each of the two subproblems is discretized by finite elements and the fluid-structure coupling is reduced to an interface boundary condition. Several numerical examples are presented and the results from the numerical computations are used to perform permeability computations for different geometries.
Keywords: fluid-structure interaction, deformable porous media, upscaling, linear elasticity, stokes, finite elements
(23 pages, 2004)

66. F. Gaspar, O. Iliev, F. Lisbona, A. Naumovich, P. Vabishchevich

On numerical solution of 1-D poroelasticity equations in a multilayered domain

Finite volume discretization of Biot system of poroelasticity in a multilayered domain is presented. Staggered grid is used in order to avoid nonphysical oscillations of the numerical solution, appearing when a collocated grid is used. Various numerical experiments are presented in order to illustrate the accuracy of the finite difference scheme. In the first group of experiments, problems having analytical solutions are solved, and the order of convergence for the velocity, the pressure, the displacements, and the stresses is analyzed. In the second group of experiments numerical solution of real problems is presented.
Keywords: poroelasticity, multilayered material, finite volume discretization, MAC type grid
(41 pages, 2004)

Status quo: November 2004